JAERI - M
89-082

VERIFICATION STUDY OF A THREE-DIMENSIONAL LOCAL SCALE ATMOSPHERIC MODEL PHYSIC AT SEACOAST REGION

June 1989

Hiromi YAMAZAWA

日 本 原 子 力 研 究 所
Japan Atomic Energy Research Institute

JAERI-Mレポートは，日本原子力研究所が不定期に公刊している研究報告書です。
入手の問合わせは，日本原子力研究所技術情報部情報資料課（〒319-11茨城県那珂郡東海村）あて，お申しこしください。なお，このほかに財団法人原子力弘済会資料センター（〒319-11 茨城県那珂郡東海村日本原子力研究所内）で複写による実費頒布をおこなっております。

JAERI-M reports are issued irregularly.
Inquiries about availability of the reports should be addressed to Information Division, Department of Technical Information, Japan Atomic Energy Research Institute, Tokai-mura, Naka-gun, Ibaraki-ken 319-11, Japan.

編集兼発行　日本原子力研究所
印　　刷　㈱原子力資料サービス

JAERI-M 89-082

Verification Study of a Three-Dimensional Local Scale Atmospheric Model PHYSIC at Seacoast Region

Hiromi YAMAZAWA

Department of Environmental Safety Research
Tokai Research Establishment
Japan Atomic Energy Research Institute
Tokai-mura, Naka-gun, Ibaraki-ken

(Received May 31, 1989)

The performance of a three-dimensional numerical atmospheric model (PHYSIC) was examined over a seacoast region with the data observed during the field tracer experiment at the Tokai site. The main frame of PHYSIC is made up of the momentum equations with the hydrostatic and Boussinesq approximation, the second-order turbulence closure model level 2.5 by Yamada and other basic equations of physical processes in the atmosphere. A terrain following z_* coordinate system is used.

The present model successfully predicts the temporal change of wind field within twenty hours from the evening to the next noon. The occurrence and structure of sea breeze are simulated satisfactorily. The model performance concerning the eddy diffusivities is thought to be reasonable, although the direct comparison between the calculation and observation is restricted to the wind and temperature profiles by the limited observation data. This was supported by an additional calculation with a diagnostic model of turbulence quantities.

Keywords: Atmospheric Model, Local Scale, Mesoscale, Turbulence Closure Model, Numerical Simulation, Sea Breeze, Coastal Region, Complex Terrain

JAERI－M　89－082

3次元局地スケール気象モデルPHYSICの沿岸域での性能検証

日本原子力研究所東海研究所環境安全研究部
山澤　弘実

（1989年5月31日受理）

大気中の移流・拡散評価に用いることを目的とした3次元数値気象モデル（PHYSIC）を開発した。このモデルは，静水圧近似及びブジネスク近似を用いた運動方程式，2次オーダーの乱流クロージャーモデルを中心とした大気中の物理過程を表わす方程式系から成る。

1983年に東海サイト周辺で実施された大気拡散実験時の気象データを用いて，沿岸域でのモデルの性能評価を行った。その結果，夕方から翌日正午までの20時間の風速場の時間変化，海風の発生とその構造をこのモデルにより再現することができた。計算と観測の直接比較は風速及び気温に限られたが，診断型モデルによる追計算により，海風発生時の乱流拡散係数の分布に関する計算結果も妥当であることが示された。

東海研究所：〒319－11　茨城県那珂郡東海村白方字白根2－4

List of symbols

A	:	albedo of ground surface
f	:	Coriolis parameter
G_0	:	conductive hear flux at ground surface
g	:	gravitational acceleration
H	:	substantial top of model
$\bar{H}$	:	top of model in z_* coordinates system
H_0	:	sensible heat flux at ground surface
K_H	:	vertical eddy diffusivity of heat
K_M	:	vertical eddy diffusivity of momentum
K_x, K_y, K_{xy}	:	horizontal eddy diffusivities
l	:	turbulence length scale
lE_0	:	latent heat flux at ground surface
q^2	:	twice of turbulence kinetic energy
S	:	solar radiation at a slope
T_{sfc}	:	ground surface temperature
u, v	:	horizontal wind components
u_g, v_g	:	geostrophic wind components
w_*	:	vertical wind velocity in z_*-coordinates system
z_g	:	ground elevation from model bottom
β	:	thermal expansion coefficient ($= \Theta_0^{-1}$)
Γ_T	:	potential temperature gradient at model top
$\delta_t, \delta_x, \delta_y, \delta_{z_*}$	:	time increment and grid intervals
ε	:	emissivity of ground surface
η	:	$(= \bar{H}/(H-z_g))$
Θ_0	:	potential temperature of reference state
θ	:	potential temperature deviation from reference state
σ_θ	:	radiative cooling/heating rate

Contents

目　　次

1. Introduction

Through the recent study to improve capability of SPEEDI (System for Prediction of Environmental Emergency Dose Information)[1], a three-dimensional numerical atmospheric model PHYSIC (Prognostic HYdroStatic model Including Closure model) was developed[2]. This model has two conspicuous characteristics; it is a prognostic model and it can simulate various phenomena such as a land-sea breeze. These characteristics are very advantageous to SPEEDI because the model can predict the meteorological situation without a dense observation network. To employ this model in the atmospheric transport and diffusion evaluation system, the performance of this model over various terrains and in various meteorological conditions must be examined.

In this report, the performance of this model over a coastal region is discussed by making use of the observation data acquired in the field tracer experiments around the Tokai site in 1983. In a coastal region, a thermal internal boundary layer (TIBL) caused by a sea breeze is seen, in which the diffusion of contaminants is much different from that in the mixing layer. The TIBL is a unstable layer with the vigorous diffusion and is capped by a stable layer. The depth of TIBL increases with the increase of distance from coastline. The development of TIBL occurs mainly in the horizontal direction with the sea breeze front invading into the inland area, whereas the development of mixing layer occurs in the vertical direction. Coexistence of these two phenomena makes the transport/diffusion process complex. Therefore, PHYSIC must be examined under such the conditions. The main outputs of this model are the three-dimensional distributions of wind and turbulence. Since these are directly used in the transport and diffusion calculation, the comparison of these items between calculation and observation are made.

2. Model

A detailed description of the model PHYSIC can be found in the previous report[2], so only an outline of it is presented here. This model consists of five prognostic equations of horizontal wind speed components (u and v), potential temperature deviation (θ), turbulence kinetic energy (q^2) and turbulence length scale (multiplied by turbulence kinetic energy as $q^2 l$). These equations are written in a terrain following z_* coordinate system. Its relation to the cartesian coordinate system is

$$z_*=\overline{H}(z-z_g)(H-z_g)^{-1} \tag{1}$$

and the horizontal coordinates are the same in the both systems.

The horizontal momentum equations in the z_* coordinate system are given by

$$\frac{Du}{Dt}=f(v-v_g)+\beta g\hat{\theta}\left(1-\frac{z_*}{\overline{H}}\right)\frac{\partial z_g}{\partial x}+\eta^2\frac{\partial}{\partial z_*}\left(K_M\frac{\partial u}{\partial z_*}\right)+\frac{\partial}{\partial x}\left(K_x\frac{\partial u}{\partial x}\right)+\frac{\partial}{\partial y}\left(K_{xy}\frac{\partial u}{\partial y}\right), \tag{2}$$

$$\frac{Dv}{Dt}=-f(u-u_g)+\beta g\hat{\theta}\left(1-\frac{z_*}{\overline{H}}\right)\frac{\partial z_g}{\partial y}+\eta^2\frac{\partial}{\partial z_*}\left(K_M\frac{\partial v}{\partial z_*}\right)+\frac{\partial}{\partial x}\left(K_{xy}\frac{\partial v}{\partial x}\right)+\frac{\partial}{\partial y}\left(K_y\frac{\partial v}{\partial y}\right), \tag{3}$$

where the operator D/Dt is defined as follows,

$$\frac{D}{Dt}=\frac{\partial}{\partial t}+u\frac{\partial}{\partial x}+v\frac{\partial}{\partial y}+\omega_*\frac{\partial}{\partial z_*}. \tag{4}$$

The continuity equation in the z_* coordinate system is expressed as follows,

$$\frac{\partial u}{\partial x}+\frac{\partial v}{\partial y}+\frac{\partial \omega_*}{\partial z_*}-(H-z_g)^{-1}\left(u\frac{\partial z_g}{\partial x}+v\frac{\partial z_g}{\partial y}\right)=0. \tag{5}$$

The heat energy equation is

$$\frac{D\theta}{Dt}=\eta^2\frac{\partial}{\partial z_*}\left(K_H\frac{\partial \theta}{\partial z_*}\right)+\frac{\partial}{\partial x}\left(K_x\frac{\partial \theta}{\partial x}\right)+\frac{\partial}{\partial y}\left(K_y\frac{\partial \theta}{\partial y}\right)-\sigma_\theta, \tag{6}$$

where σ_θ is the radiative cooling rate that is expressed by the Newtonian cooling using the temperature difference between the air and the ground surface.

A second-order turbulence closure model developed by Yamada[3] is used to close

the turbulence quantities in the momentum equations and the heat energy conservation equation. This turbulence closure model prognostically calculate the turbulence kinetic energy and turbulence length scale. It is possible to calculate the eddy diffusivities as well as other turbulence quantities, e.g. $\overline{w'^2}, \overline{u'^2}, \overline{v'^2}$ etc., directly from the prognostically calculated quantities. The turbulence kinetic energy equation and turbulence length scale equation are as below,

$$\frac{Dq^2}{Dt}=\eta^2\frac{\partial}{\partial z_*}\left(K_q\frac{\partial q^2}{\partial z_*}\right)+\frac{\partial}{\partial x}\left(K_x\frac{\partial q^2}{\partial x}\right)+\frac{\partial}{\partial y}\left(K_y\frac{\partial q^2}{\partial y}\right)+P_q+D_q, \tag{7}$$

$$\frac{Dq^2l}{Dt}=\eta^2\frac{\partial}{\partial z_*}\left(K_q\frac{\partial q^2l}{\partial z_*}\right)+\frac{\partial}{\partial x}\left(K_x\frac{\partial q^2l}{\partial x}\right)+\frac{\partial}{\partial y}\left(K_y\frac{\partial q^2l}{\partial y}\right)+P_l+D_l, \tag{8}$$

where P_q and P_l are the production terms of q^2 and q^2l, and D_q and D_l are the dissipation terms.

The soil temperature T_s is calculated by solving the heat conduction equation, i.e.,

$$\frac{\partial T_s}{\partial t}=\frac{\partial}{\partial z_s}\left(k_s\frac{\partial T_s}{\partial z_s}\right), \tag{9}$$

where k_s is the thermal conductivity of soil and the suffix s denotes variables of the soil layer. The ground surface temperature which is the boundary condition of Eqs. (6) and (9) is calculated by the heat budget equation, i.e.,

$$\varepsilon(L\downarrow-\sigma T_{sfc}^4)+(1-A)S=H_0+lE_0+G_0, \tag{10}$$

where ε and A are the emissivity and albedo of ground surface, respectively, and $L\downarrow$ the downward long-wave radiation, S the solar radiation, and H_0, lE_0 and G_0 are the sensible heat flux, latent heat flux and conductive heat flux at the ground surface, respectively.

The time integration is performed by using the Alternating Direction Implicit (A.D.I.) method. This method has been applied to an atmospheric numerical model

by Yamada[3] . The boundary conditions are as follows. The lateral boundary condition is given by the radiation condition, i.e.,

$$\frac{\partial \varphi}{\partial t} + c\frac{\partial \varphi}{\partial n} = 0 \ , \tag{11}$$

where $\partial\varphi/\partial n$ is the differentiation of φ in the direction normal to the lateral boundary and c is the phase velocity calculated from the values at inner grid points. The top boundary conditions are as follows,

$$\frac{\partial u}{\partial z_*} = \frac{\partial v}{\partial z_*} = 0, \tag{12}$$

$$\frac{\partial \Theta}{\partial z_*} = \Gamma_T, \tag{13}$$

$$q^2 = q^2 l = 0, \tag{14}$$

where Γ_T is the potential temperature gradient at the top of model and its typical value is 3.5℃/km. The lowest grid level of the model is set in the surface layer. The bottom boundary conditions are given by the surface layer formulae based on the Monin-Obukhov similarity theory.

3. Calculation condition

3.1 Meteorological data

Six series of atmospheric diffusion experiments were carried out to provide the verification data for SPEEDI during the period from 1980 to 1985 (Kakuta and Hayashi[4),5)] and Kakuta et al.[6)]). During the first four years, the experiments were carried out around the Tokai site where the coast line is rather linear and the terrain is flat except for rolling lower than 50 m and a small mountainous area at north part of experiment area as shown in Fig. 1. During the experiment period, adding to the tracer concentration measurements, the meteorological observations were conducted. The surface wind velocity was measured every hour at fifteen points. The vertical profiles of wind velocity and temperature were measured at three points for the rawinsonde observation and at an additional point for the pilot balloon observation. The surface observation of temperature, humidity, solar radiation and net radiation were carried out at the release point (RLP). The comparison of wind field, its temporal change and vertical temperature profiles between the observation and calculation will be discussed in the following chapter.

The calculation covers the situation in the period from the evening of August 7, 1983 to the next noon (TOKAI 83). Since the experiment area was situated in a high pressure area in this period, the synoptic wind was very weak. The cloudiness was less than a tenth in this period. It was thus favorable to the development of a sea breeze.

3.2 Numerical aspects

The calculation domain is 30 km × 30 km × 2.2 km (Fig. 1) and it is divided into 31×31×16 grid points. The calculation parameters are chosen as follows;

calculation period: 20 hours from 1600 JST, 7 Aug., 1983 to the next noon,

time increment: 30 s,

horizontal grid interval: 1 km,

albedo of land surface: 0.25,

heat conductivity of soil: 0.2 W $m^{-1}K^{-1}$,

Coriolis parameter: 0.865 $\times 10^{-4}$ s^{-1} (latitude $\varphi=36.5°N$).

The vertical grid heights are listed in Table 1. The roughness parameter z_0 is determined on the basis of the land surface utilization[7]. The roughness parameters of potential temperature and specific humidity, z_θ and z_q respectively, are assumed as

$$z_\theta = z_q = z_0 \exp(-kB_H^{-1}), \tag{15}$$

where $B_H^{-1}=5$.

The initial condition of wind velocity is the wind profile observed at the initial time at RLP (Fig. 2) and its horizontal uniformity is assumed. Since the potential temperature profile at the initial time was not observed, its initial condition is assumed as

$$\theta = \theta_{sfc} + \Gamma z, \tag{16}$$

where $\theta_{sfc}=31℃$ and $\Gamma=3.0℃/km$. The horizontal uniformity of potential temperature all over the calculation area is also assumed. The initial surface temperatures are 31 ℃ at the ground surface and 19 ℃ at the sea surface. The initial soil temperature is assumed to be constant with depth and equal to the surface temperature. The sea surface temperature is fixed to the initial value throughout the calculation. The specific humidity at the lowest level (z_*= 5 m) is treated as a constant (18.0 g/kg) because its temporal change observed during the calculation period was no more than 0.2 g/kg. Figure 3 depicts the external pressure gradient with respect to the horizontal direction applied at the model top in terms of the geostrophic wind velocity. This pressure gradient is determined

to make the calculated wind velocity at z = 1000m over RLP (release point) at 0900 JST (Japan Standard Time) coincide with the observed one. The upper limits of eddy diffusivities are set to 60 m^2/s and 75 m^2/s for K_M and K_H, respectively, so as to keep the turbulence quantities within a reasonable range.

4. Results

4.1 Temporal change of surface wind

Figure 4 depicts the temporal changes of surface wind direction and speed at six observation points (solid lines). The observed data were recorded every hour so that the calculation results are plotted at the same interval (dashed lines). The observed wind speed is an adjusted value at z = 5 m.

The observed wind gradually rotated from the southwest in the evening of the first day to the northwest in the next early morning. This situation was the same at all observation points except for OKD (Okada) which was located at the foot of mountain in the northern part of calculation area. The wind speed decreased from 3 to 4 m/s at the initial time to calm, which is less than 0.5 m/s, within 3 to 6 hours and remained calm till dawn. These temporal changes of wind direction were simulated considerably well. Although the discrepancy of wind direction between calculation and observation at HTC (Hitachi) at 2200 JST seems quite large, it is not serious because the fluctuation was caused by sign changes of u component and its absolute value was small. Generally speaking, the calculated wind speed decreased rapidly in the evening as compared with the observed one. It is the reason for this result that the initial surface wind speed was less than observed one and the initial vertical profile of potential temperature was steep. The stability in late afternoon is usually near-neutral, but there was no observation of vertical distribution of potential temperature at that time. Therefore, these initial

to make the calculated wind velocity at z = 1000m over RLP (release point) at 0900 JST (Japan Standard Time) coincide with the observed one. The upper limits of eddy diffusivities are set to 60 m^2/s and 75 m^2/s for K_M and K_H, respectively, so as to keep the turbulence quantities within a reasonable range.

4. Results

4.1 Temporal change of surface wind

Figure 4 depicts the temporal changes of surface wind direction and speed at six observation points (solid lines). The observed data were recorded every hour so that the calculation results are plotted at the same interval (dashed lines). The observed wind speed is an adjusted value at z = 5 m.

The observed wind gradually rotated from the southwest in the evening of the first day to the northwest in the next early morning. This situation was the same at all observation points except for OKD (Okada) which was located at the foot of mountain in the northern part of calculation area. The wind speed decreased from 3 to 4 m/s at the initial time to calm, which is less than 0.5 m/s, within 3 to 6 hours and remained calm till dawn. These temporal changes of wind direction were simulated considerably well. Although the discrepancy of wind direction between calculation and observation at HTC (Hitachi) at 2200 JST seems quite large, it is not serious because the fluctuation was caused by sign changes of u component and its absolute value was small. Generally speaking, the calculated wind speed decreased rapidly in the evening as compared with the observed one. It is the reason for this result that the initial surface wind speed was less than observed one and the initial vertical profile of potential temperature was steep. The stability in late afternoon is usually near-neutral, but there was no observation of vertical distribution of potential temperature at that time. Therefore, these initial

conditions caused stronger stability in the evening and made the calculated surface wind speed weaker than the observed one.

In the early morning after sunrise, increases in wind speeds at RLP and SGY (Sugaya) were observed. It is considered that this phenomenon was caused by the development of unstable layer and the entrainment of upper layer where the wind from the northwest was stronger than in the surface layer. The present model failed to simulate this phenomena. The model calculation actually showed the entrainment of upper layer as shown by the development of unstable layer and the slight increase in wind speed (Fig. 4) but the wind speed at higher level was not strong enough to make the surface wind speed as observed. It is considered that the rather strong wind, which was not simulated by PHYSIC, was caused by the surrounding topography that is just outside the calculation area.

During the period from 0500 to 1000 JST, sudden changes of wind direction showing the passage of sea breeze front were observed at all observation points. The calculation results showed good agreement with the observed data. The times of sea breeze front passage in the morning are summarized in Table 2. The observation times listed in Table 2 are the initial times of wind direction changes, for instance at RLP, the wind direction change was observed during the period from 0700 to 0800 JST. Excellent correspondence between observation and calculation is seen except for OKD. At OKD, a sudden change in wind direction was not detected both by the calculation and observation. Both the calculation and observation showed that the passage time of sea breeze front, except for one at HTC, was delayed according to the distance from coastline. At HTC, the wind direction change was observed earlier than RLP. This is because the observation point HTC is situated at the foot of mountain. So, a upslope flow took place and merged with sea breeze.

This situation was successfully simulated. The differences of sea breeze front passage time and wind direction between the calculation and observation are, respectively, at most 1 h and 45°, respectively.

4.2 Spatial distribution of wind velocity

Figure 5 depicts the horizontal distribution of calculated and observed surface wind. The scales of arrows are different between the observation and calculation. Downslop flows were calculated at the mountainous region in the early morning. According to the calculation, the sea breeze occurred before 0800 JST, and invaded 3 km inland at 0800 JST and 9 km at 0900 JST. The distortion of sea breeze at the mountainous area are clearly shown. These were well supported by the observation. The discrepancy of wind direction of sea breeze at 0800 JST is thought to be caused by the strong northwest wind as mentioned in the previous section (4.1). Figure 6 shows the horizontal distribution of wind velocity at the level z_*=84 and 314 m together with the wind velocity observed with pilot balloons. These figures show excellent agreements of wind velocity both in the sea breeze region and in its frontal area where the wind direction was different from that in the sea breeze region and the wind speed was weaker (Fig. 6－(b)). As shown in Fig. 5－(i), the north wind at the northwest corner of the calculation area remained till noon. This was because the north boundary condition was the radiation condition which was not suitable for the inflow boundary where a mixing layer was developing.

Figure 7 depicts the comparison of vertical wind profiles between observation and calculation. At RLP, the general shapes of profiles fairly agree with the observations. However, the gentle peak of wind speed observed at the layer between 200 and 500 m was not calculated. The observed and calculated wind profiles at

SGY showed a low level peak at z_*= 100 to 200 m and a weak wind layer around z_*= 400 m. These were the sea breeze and its counter flow layer, respectively, but the general wind made the counter flow obscure. At OKD, discrepancy of wind direction is seen. The observed wind was blowing into a valley just north of calculation area, although the calculated wind was blowing toward the west having the original direction of sea breeze. It is considered that, in order to accurately simulate the wind field around the mountain at the north part of calculation area, the expansion of calculation area is necessary.

4.3 Potential temperature and eddy diffusivity

The developments of mixing layer and sea breeze are shown in Fig. 8, which depicts the distributions of wind velocity (u,w) and potential temperature together with the eddy diffusivity in the vertical cross section along the line B in Fig. 1 from 0600 to 1200 JST. The light and thick hatched areas express the regions where 1 $\leqq K_M <$ 10 m^2/s and $K_M \geqq$ 10 m^2/s, respectively. The depth of the mixing layer, which can be identified with the top of thick hatched area, increased with time. With the invasion of sea breeze, the developing mixing layer became shallow and was capped by a stable layer, becoming a thermal internal boundary layer (TIBL). The calculation also showed the dependency of TIBL depth on the distance from coastline (fetch l_f). At noon, the depth of TIBL was about 100 m at l_f = 5 km, 200 m at l_f = 10 km and 300 m at l_f = 15 km.

The development of mixing layer and the invasion of sea breeze at the mountainous area were more complex. Figure 9 shows the distributions of wind velocity, potential temperature and eddy diffusivity in the cross section along line A in Fig. 1. At 0700 JST, upslope flows occurred on the east and west slopes of the mountain causing a convergence over the top of the mountain. The mixing layer

over the east slope was deeper than that over west slope because of the differential heating by the solar radiation. The development of mixing layer over the mountainous region was suppressed as well as over the flat region by the stable maritime air invading into the inland region. The distribution of eddy diffusivity was strongly affected by the circulation over the convergence areas where updrafts took place and the mixing layer was deep and overturning.

The comparisons of vertical profiles of potential temperature at 1100 JST are shown in Fig. 10. The calculation successfully simulated the surface inversion at RLP and the TIBL structure at HNB (Honbu). The discrepancy at upper layer above 500 m and the failure to simulate the elevated inversion between 400 and 500 m are thought to be caused by the lack of observation data of temperature profile at the initial time and the synoptic change of temperature.

The fair agreement of vertical profiles of wind velocity and potential temperature with the observed ones implies the validity of eddy diffusivity calculated. This is supported by another calculation as follows. The second-order turbulence closure model level 2.0[8] is a diagnostic model of turbulence quantities. By this model, the turbulence kinetic energy is calculated by assuming its local equilibrium, i.e. the local production and the local dissipation of turbulence energy balance each other. With this method, the vertical profiles of eddy diffusivity K_M were calculated from the profiles of wind and potential temperature observed over HNB and SGY at 1100 JST (Fig.11). Although these profiles of K_M were not observed directly, these can be regarded as observed ones as compared with the profiles calculated by PHYSIC. The good agreement of the calculated and observed profiles shown in Fig.11 indicates the validity of calculation by PHYSIC.

5. Conclusions

A three-dimensional atmospheric model was developed in order to apply it to the atmospheric transport and diffusion evaluation in the local scale atmosphere with a complex terrain. This model, PHYSIC, consists of the momentum equations with the hydrostatic and Boussinesq approximation in addition to the conservation equations of heat, turbulent kinetic energy and turbulent length scale, the heat budget equation and the heat conduction equation in the soil layer. The coordinate system is the terrain following z_* coordinate system which allows the existence of a complex terrain.

The present model was applied to simulate the sea breeze observed during the atmospheric diffusion experiments around the Tokai site in 1983. The purpose of this calculation is to examine the performance of this model at a coastal region. Most of the initial conditions were assumed because the observation data were not available. Only the vertical wind profile was observed. In spite of the lack of observed data at the initial time, PHYSIC successfully predicted the temporal change of wind field within twenty hours and the occurrence and structure of sea breeze. Although the limitation of observed data did not allow the precise comparison of turbulence field, it was considered that the calculated results of sea breeze structure concerning the eddy diffusivities were reasonable because the profiles of wind and potential temperature in TIBL (thermal internal boundary layer) were simulated well. This was supported by another calculation with a diagnostic model of the atmospheric turbulence. Therefore, it is concluded that the general performance of this model is satisfactory. However,

Acknowledgments

The author is grateful to Dr. F. Kimura and Mr. S. Takahashi of the Meteorological Research Institute, the Japan Meteorological Agency for their helpful comments on the present results. Thanks are also due to Dr. S. Moriuchi for his careful reviewing and to Messrs. M. Chino and H. Ishikawa for their useful discussion.

References

1) K. Imai et al.: "SPEEDI: A Computer Code System for the Real-Time Prediction of Radiation Dose to the Public due to an Accidental Release", JAERI 1297 (1985)

2) H. Yamazawa: "Development of a Three-Dimensional Local Scale Atmospheric Model with Turbulence Closure Model", submitted to JAERI M (1989)

3) T. Yamada: "A Three Dimensional, Second-Order Closure Numerical Model of Mesoscale Circulations in the Lower Atmosphere" Argonne National Laboratory, ANL/RER-78-1 (1978)

4) M. Kakuta and T. Hayashi: "Results of Atmospheric Diffusion Experiments Vol.1 TOKAI 80, TOKAI 81 (in Japanese)", JAERI-M 86-021 (1986)

5) M. Kakuta and T. Hayashi: "Results of Atmospheric Diffusion Experiments Vol.2 TOKAI 82, TOKAI 83 (in Japanese)", JAERI-M 86-097 (1986)

6) M. Kakuta, T. Hayashi and T. Adachi: "Results of Atmospheric Diffusion Experiments Vol.3 TOKAI 84, TOKAI 85 (in Japanese)", JAERI-M 88-024 (1988)

7) J. Kondo and H. Yamazawa: "Aerodynamic Roughness over an Inhomogeneous Ground Surface", Boundary-Layer Met., 35, 331 (1986)

8) G. L. Mellor and T. Yamada: "A Hierarchy of Turbulence Closure Models for Planetary Boundary Layer", J. Atmos. Sci., 31, 1971 (1974)

Acknowledgments

The author is grateful to Dr. F. Kimura and Mr. S. Takahashi of the Meteorological Research Institute, the Japan Meteorological Agency for their helpful comments on the present results. Thanks are also due to Dr. S. Moriuchi for his careful reviewing and to Messrs. M. Chino and H. Ishikawa for their useful discussion.

References

1) K. Imai et al.: "SPEEDI: A Computer Code System for the Real-Time Prediction of Radiation Dose to the Public due to an Accidental Release", JAERI 1297 (1985)

2) H. Yamazawa: "Development of a Three-Dimensional Local Scale Atmospheric Model with Turbulence Closure Model", submitted to JAERI M (1989)

3) T. Yamada: "A Three Dimensional, Second-Order Closure Numerical Model of Mesoscale Circulations in the Lower Atmosphere" Argonne National Laboratory, ANL/RER-78-1 (1978)

4) M. Kakuta and T. Hayashi: "Results of Atmospheric Diffusion Experiments Vol.1 TOKAI 80, TOKAI 81 (in Japanese)", JAERI-M 86-021 (1986)

5) M. Kakuta and T. Hayashi: "Results of Atmospheric Diffusion Experiments Vol.2 TOKAI 82, TOKAI 83 (in Japanese)", JAERI-M 86-097 (1986)

6) M. Kakuta, T. Hayashi and T. Adachi: "Results of Atmospheric Diffusion Experiments Vol.3 TOKAI 84, TOKAI 85 (in Japanese)", JAERI-M 88-024 (1988)

7) J. Kondo and H. Yamazawa: "Aerodynamic Roughness over an Inhomogeneous Ground Surface", Boundary-Layer Met., 35, 331 (1986)

8) G. L. Mellor and T. Yamada: "A Hierarchy of Turbulence Closure Models for Planetary Boundary Layer", J. Atmos. Sci., 31, 1971 (1974)

Table 1 Grid height in the air and grid depth in the soil.

No.	Mean variables height (m)	Turbulence variables height (m)	Soil temperature depth (m)
1	5.0	11.6	0.01
2	25.0	47.7	0.03
3	84.3	130.8	0.09
4	186.0	247.8	0.18
5	314.4	384.7	0.36
6	457.7	533.0	
7	609.0	688.3	
8	767.8	848.2	
9	929.5	1011.5	
10	1094.1	1177.2	
11	1260.8	1344.8	
12	1429.2	1513.9	
13	1598.0	1684.1	
14	1769.6	1855.3	
15	1941.2	2027.3	
16	2113.6	2200.0	

Table 2 Times (JST) of sea breeze front passage.
The fetch is the distance from coastline.

Location	Fetch (km)	Passage time (JST)	
		Calculation	Observation
RLP	0	0715	07
HTC	1	0525	05
IST	4	0810	08
ASZ	5	0825	08
SNB	7	0830	08
KTK	8	0840	08
OKD	8	——	——
SGY	10	0920	09
MIT	13	0930	09
KKN	16	1015	09

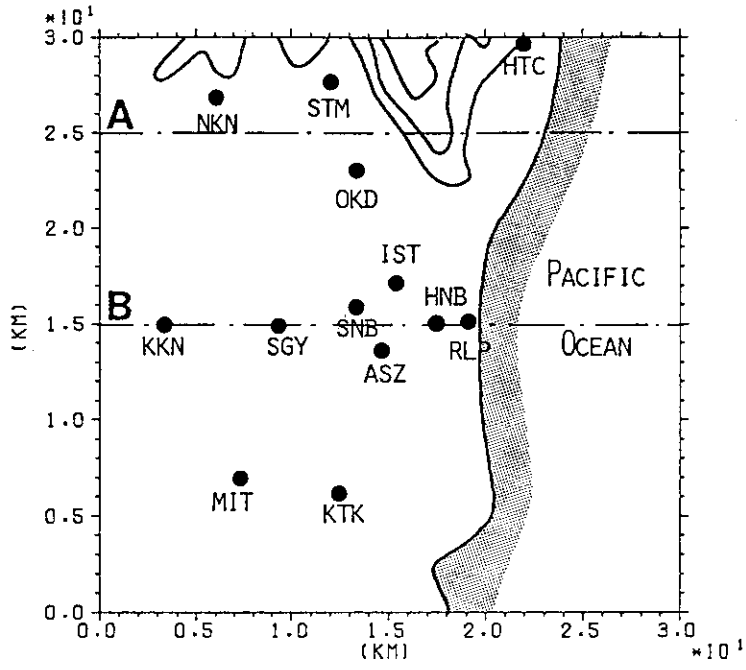

Fig. 1 Computational domain of sea breeze simulation. The values of contour lines are 100, 200 and 300 m above the sea level. The circles show the location of meteorological observation during the atmospheric diffusion experiments (Tokai 83).

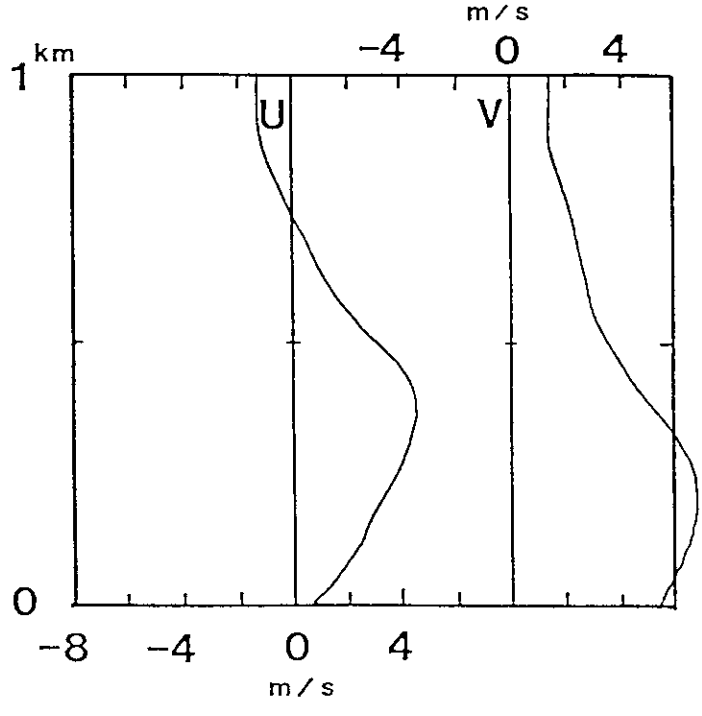

Fig. 2 Initial vertical profiles of U and V.

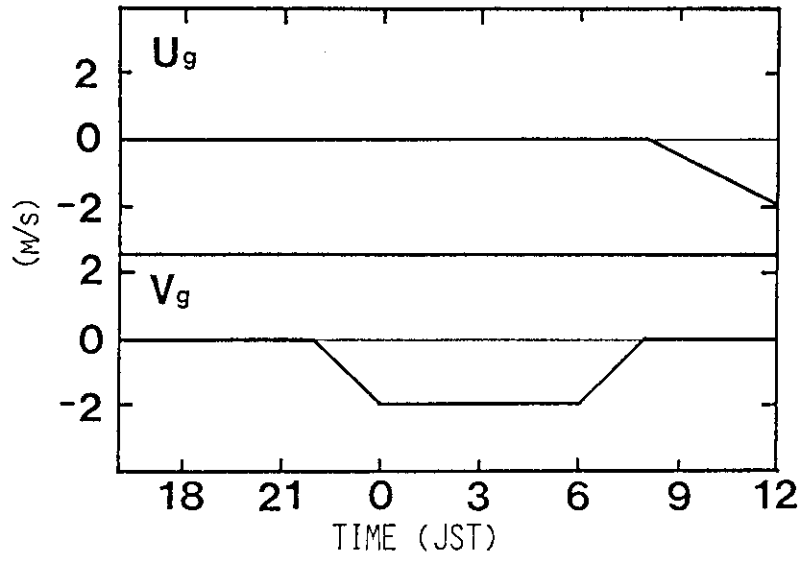

Fig. 3 Temporal pressure change applied at the model top in terms of geostrophic wind speed (U_g,V_g).

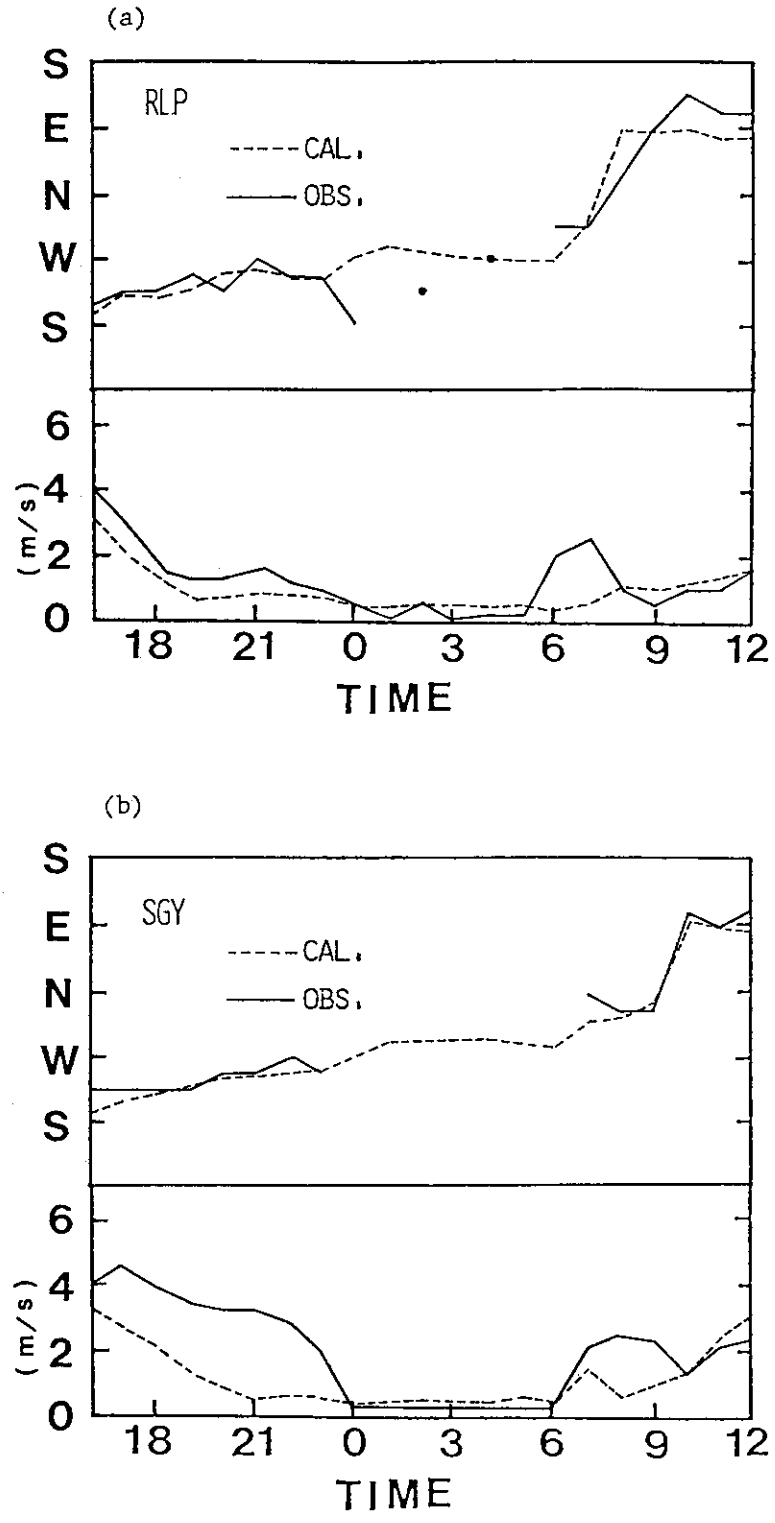

Fig. 4 Temporal change of observed and calculated surface wind. The solid and dashed lines show the observed and calculated value, respectively. The data is plotted with intervals of one hour. The blanks in the observed wind direction show that the observed wind is calm and wind direction is undefinable. The observed wind speed is an adjusted value at z=5 m.

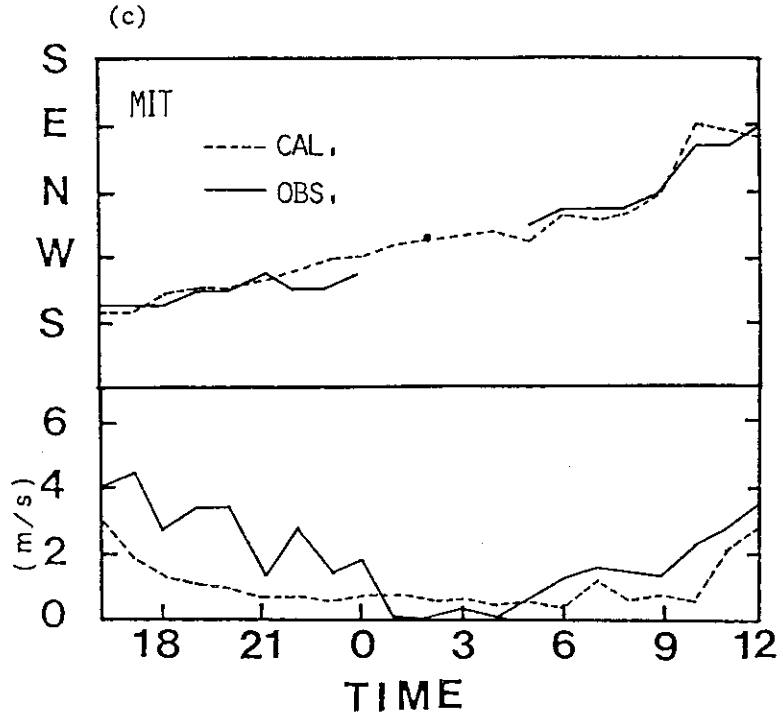

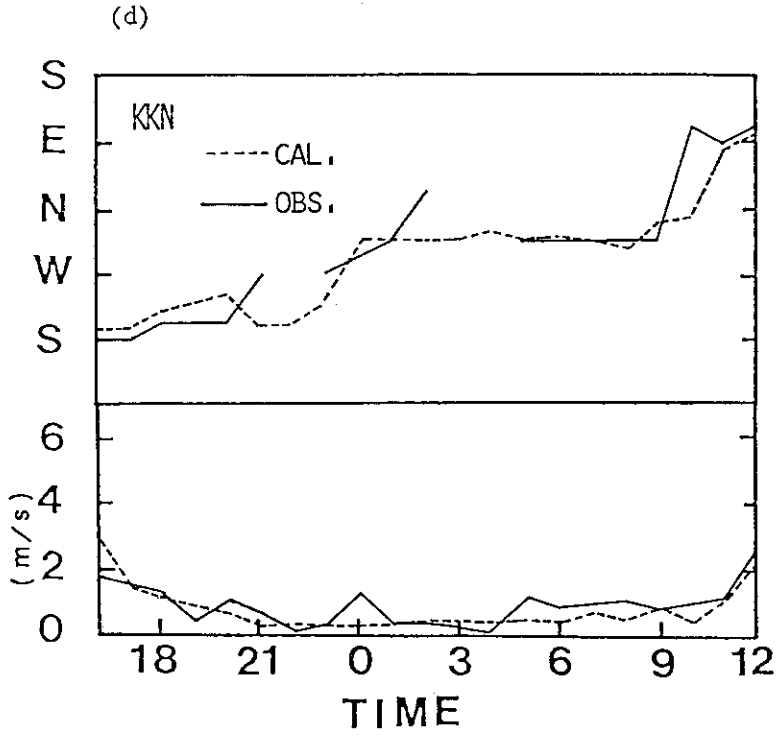

Fig. 4 (Continued)

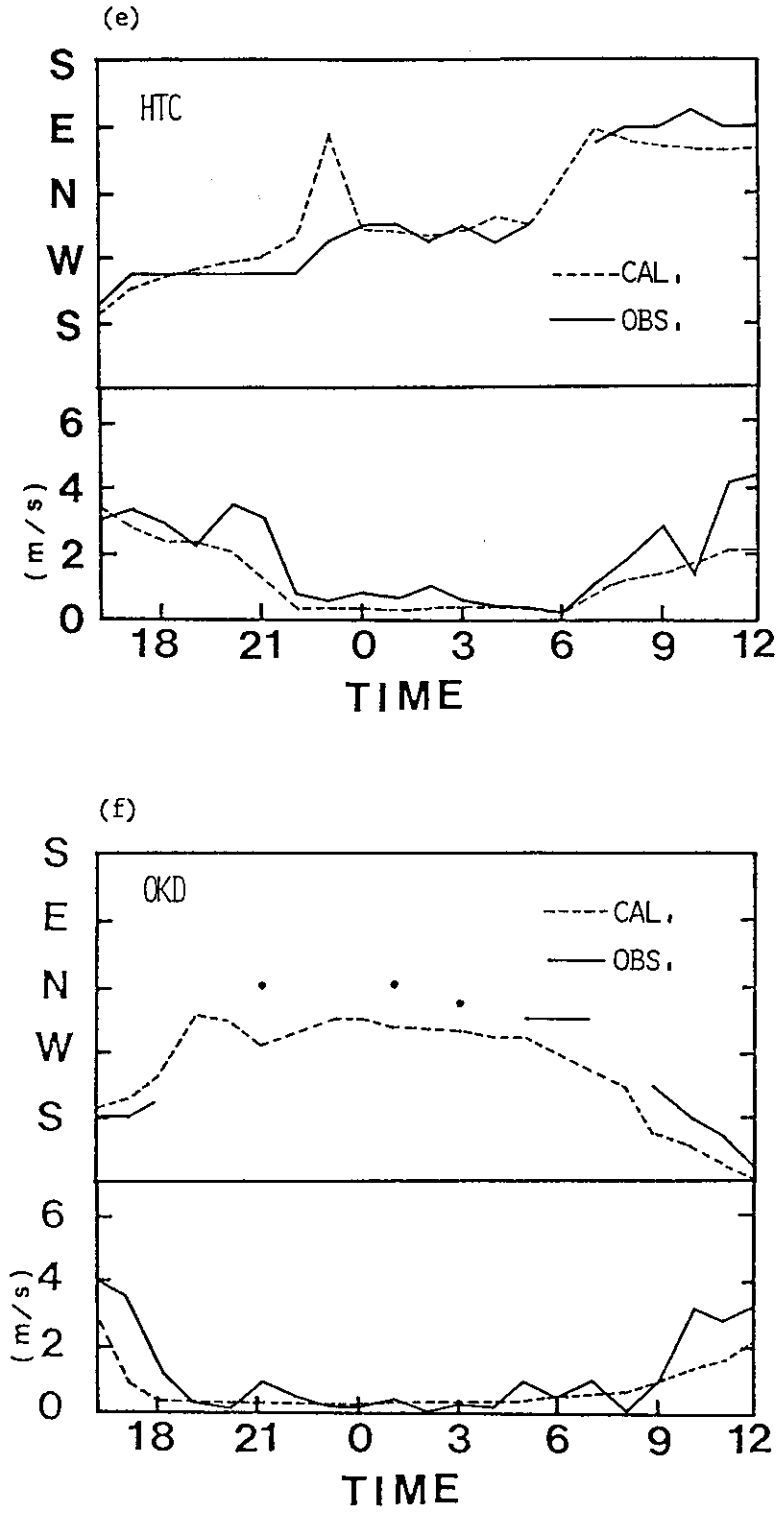

Fig. 4 (Continued)

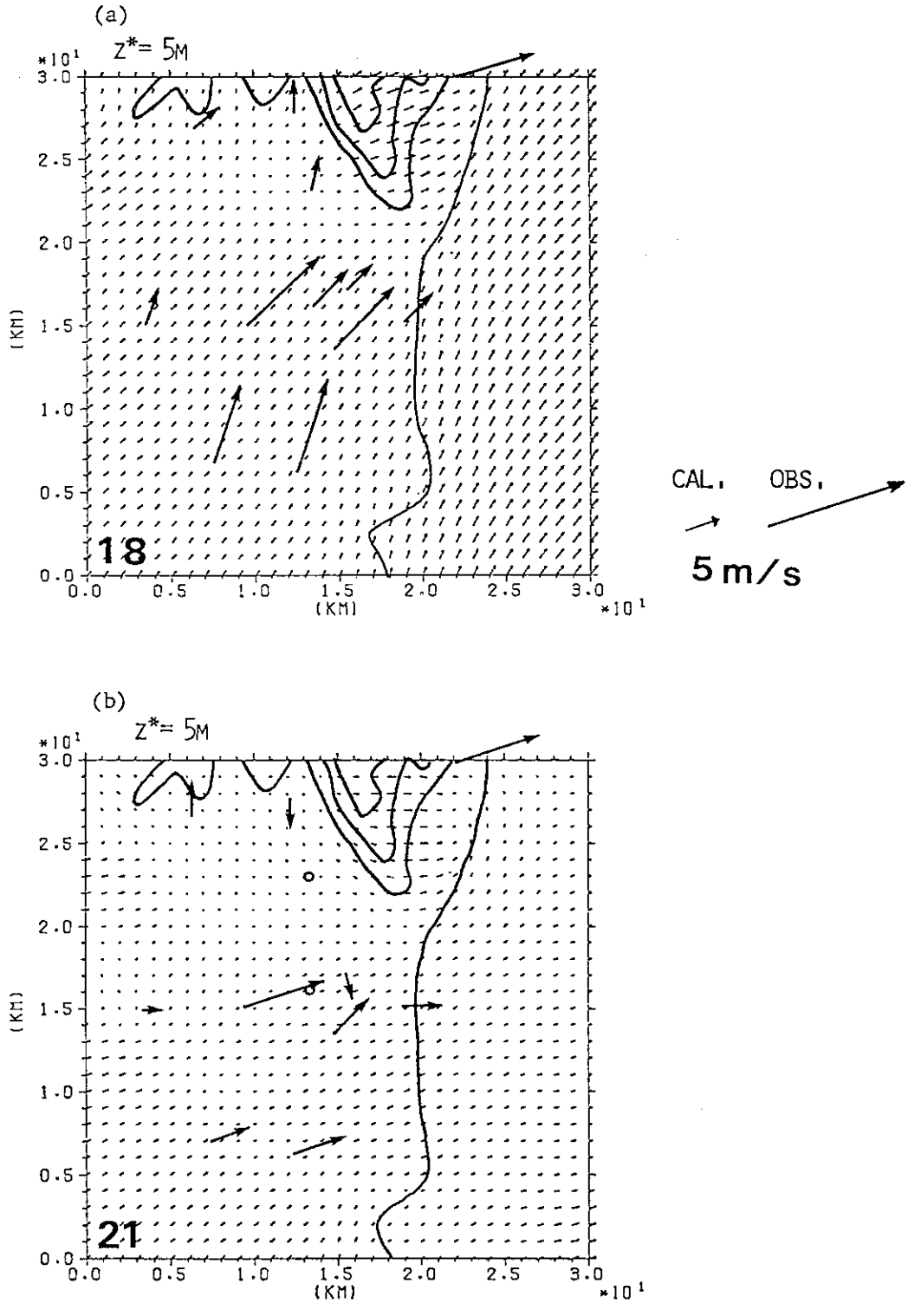

Fig. 5 Horizontal distributions of observed and calculated surface wind velocity (z_*=5 m) at 18h, 21h, 04h, 06h and 08h through 12h JST. The open circles show the observation of calm wind.

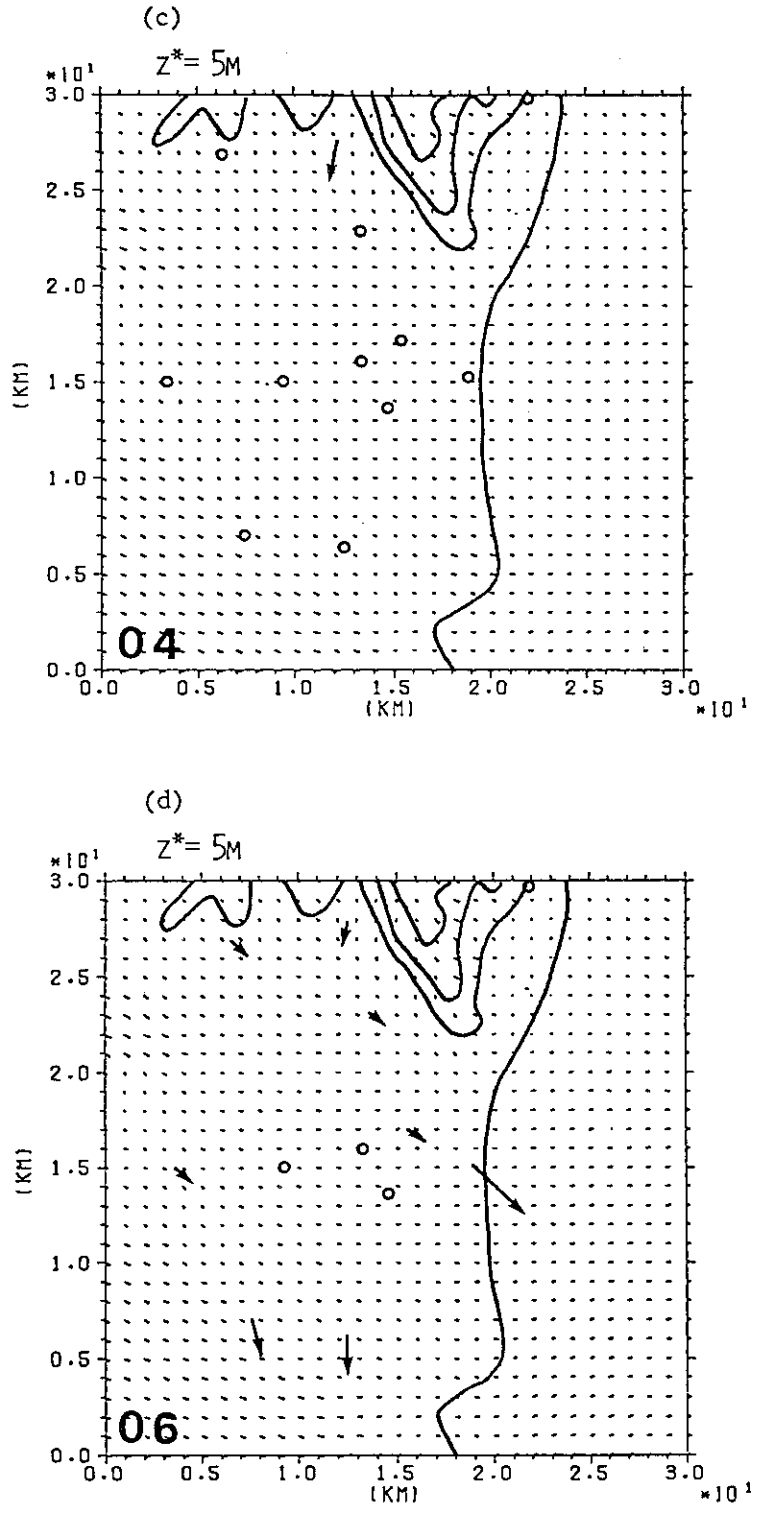

Fig. 5 (Continued)

(e)

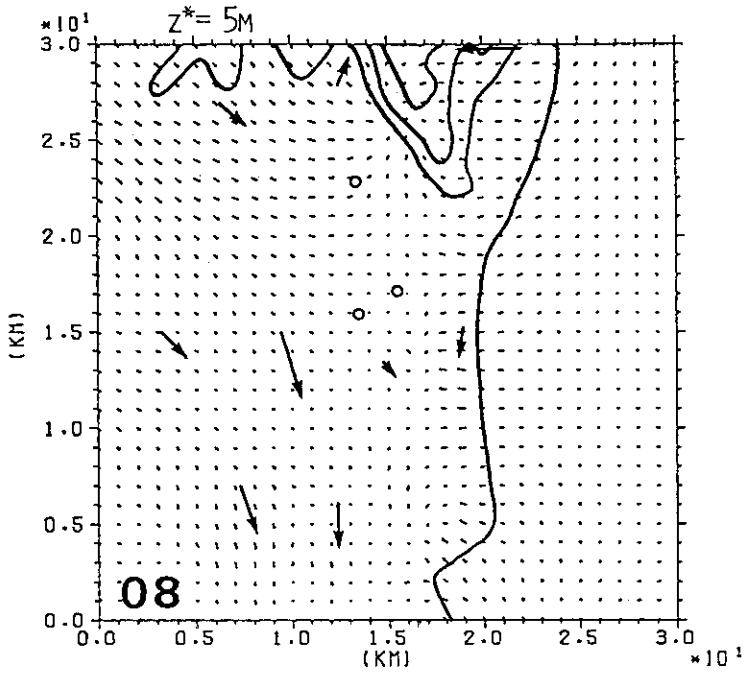

(f)

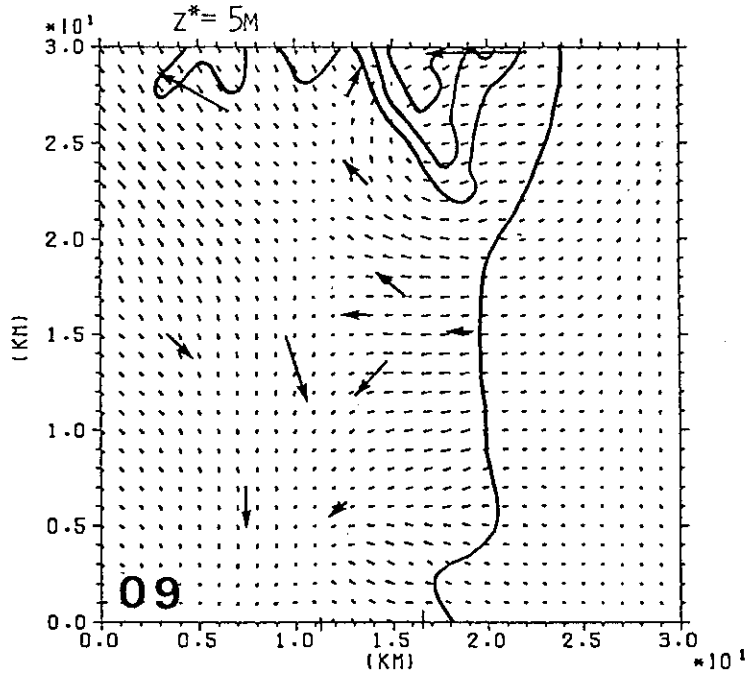

Fig. 5 (Continued)

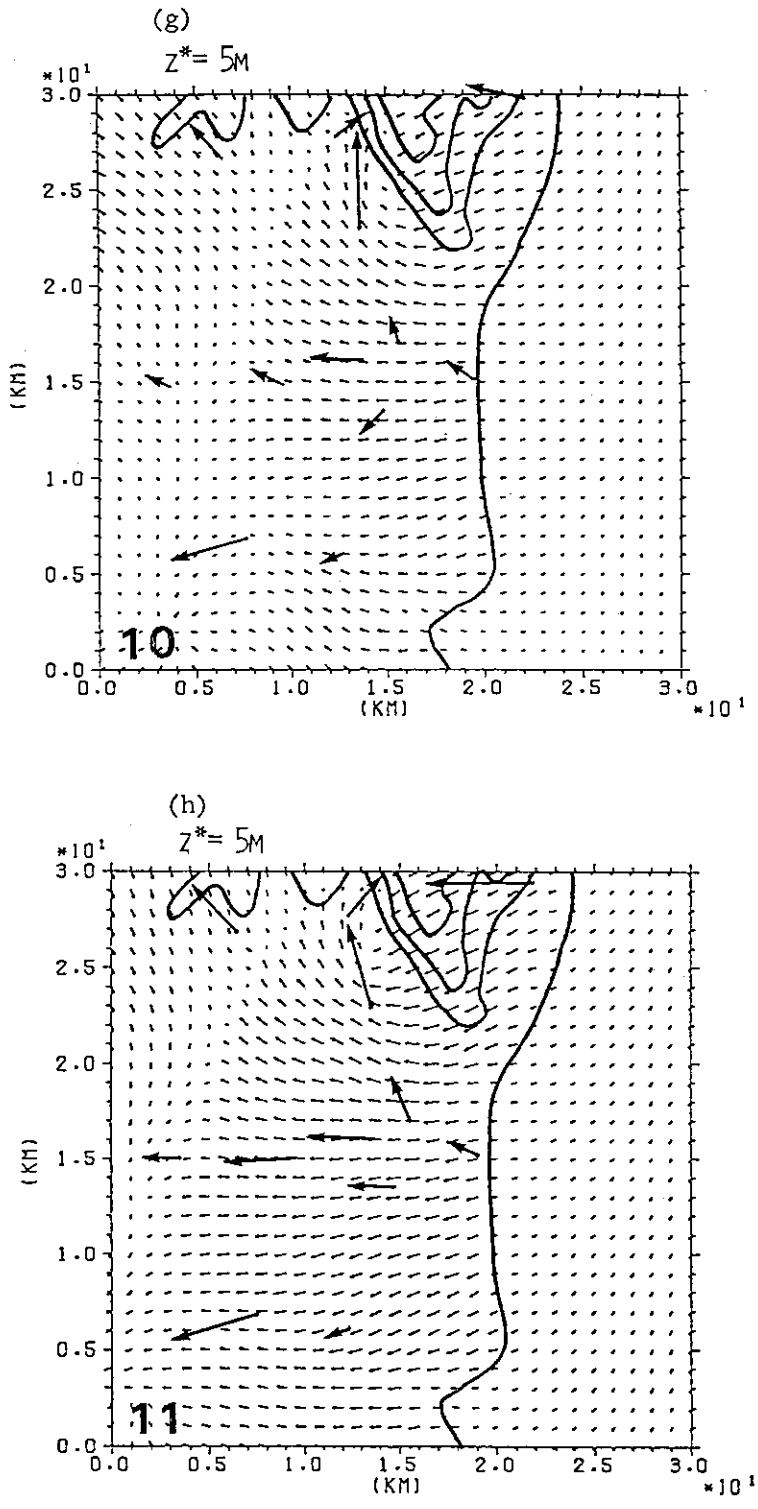

Fig. 5 (Continued)

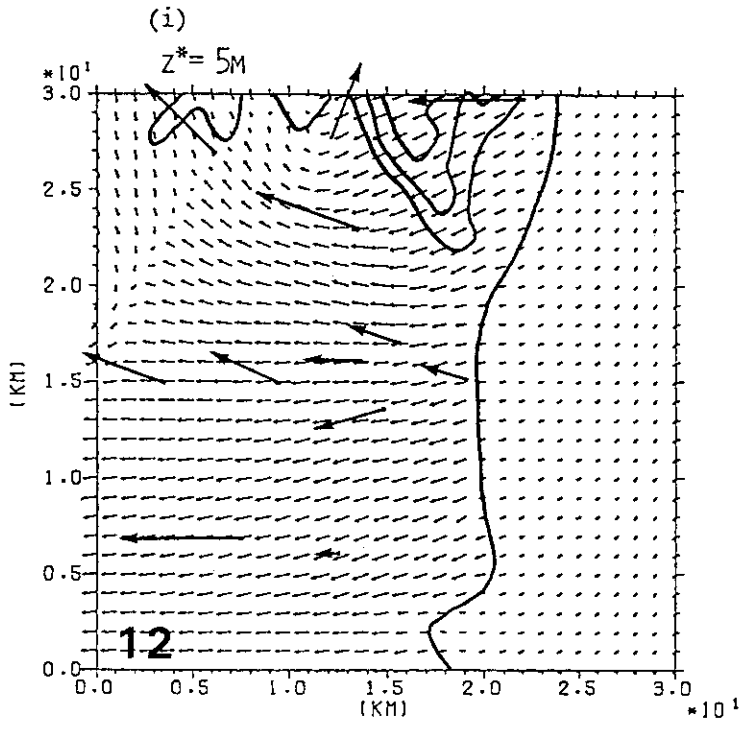

Fig. 5 (Continued)

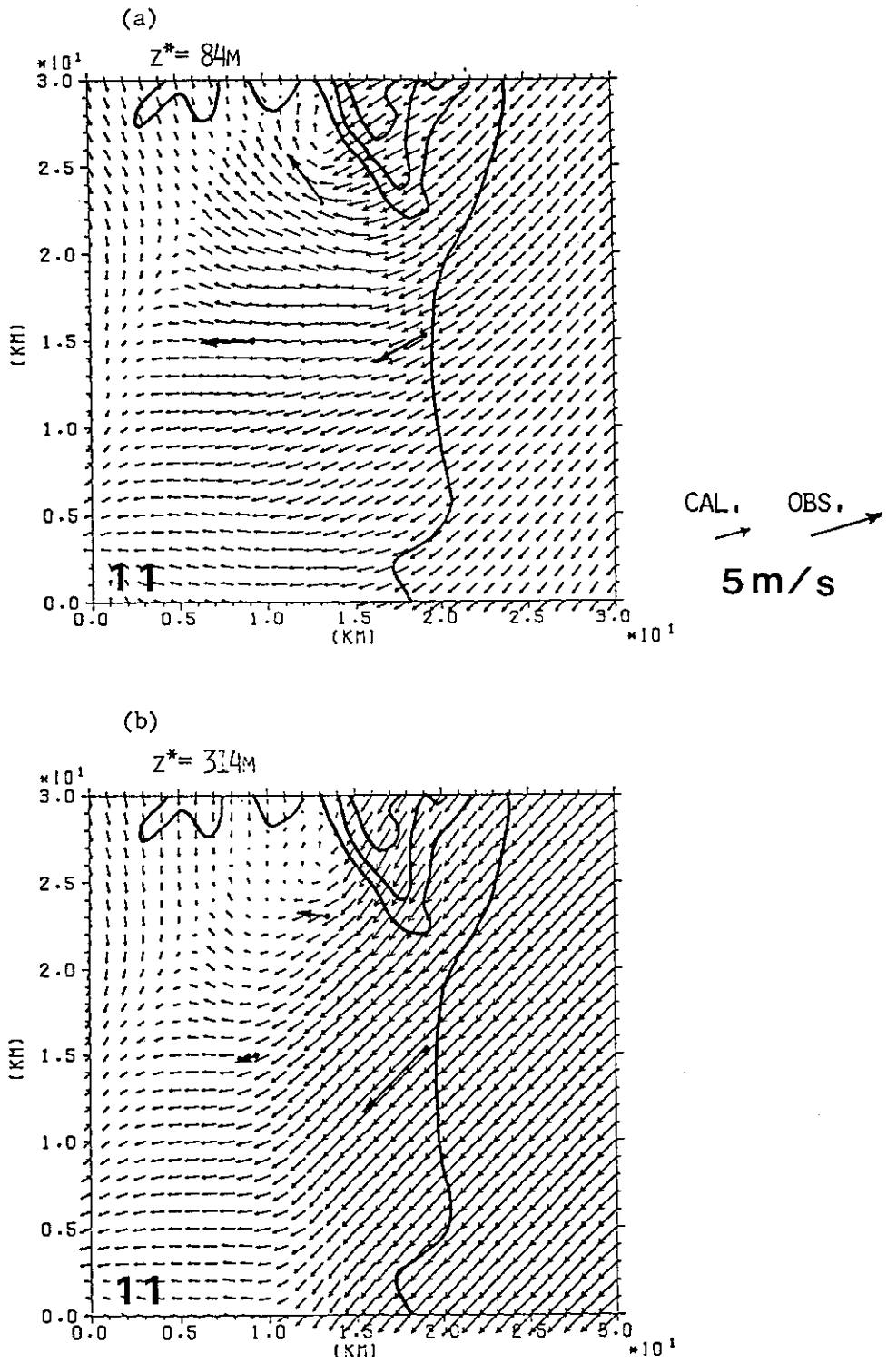

Fig. 6 Horizontal distributions of observed and calculated wind velocity at 11h (a, b) and 12h (c, d).

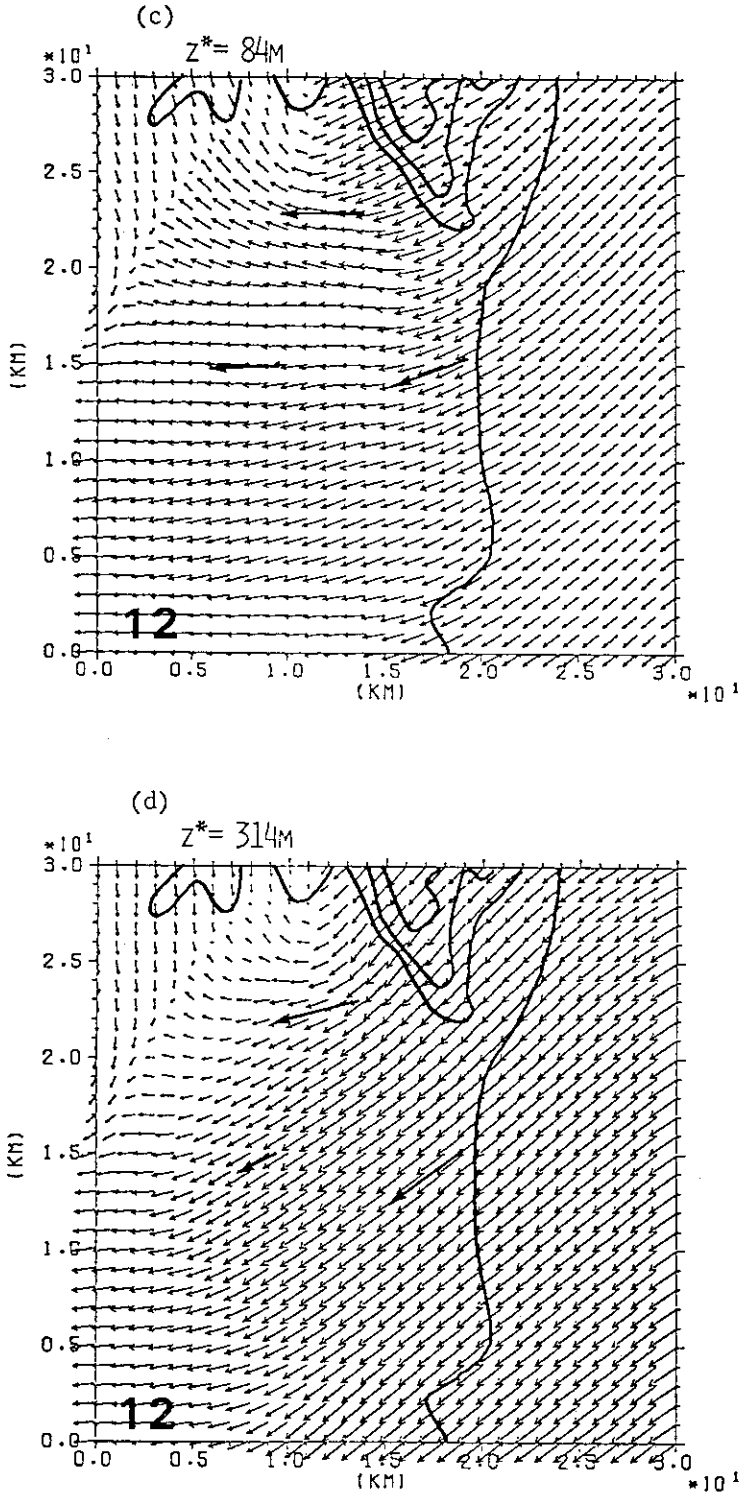

Fig. 6 (Continued)

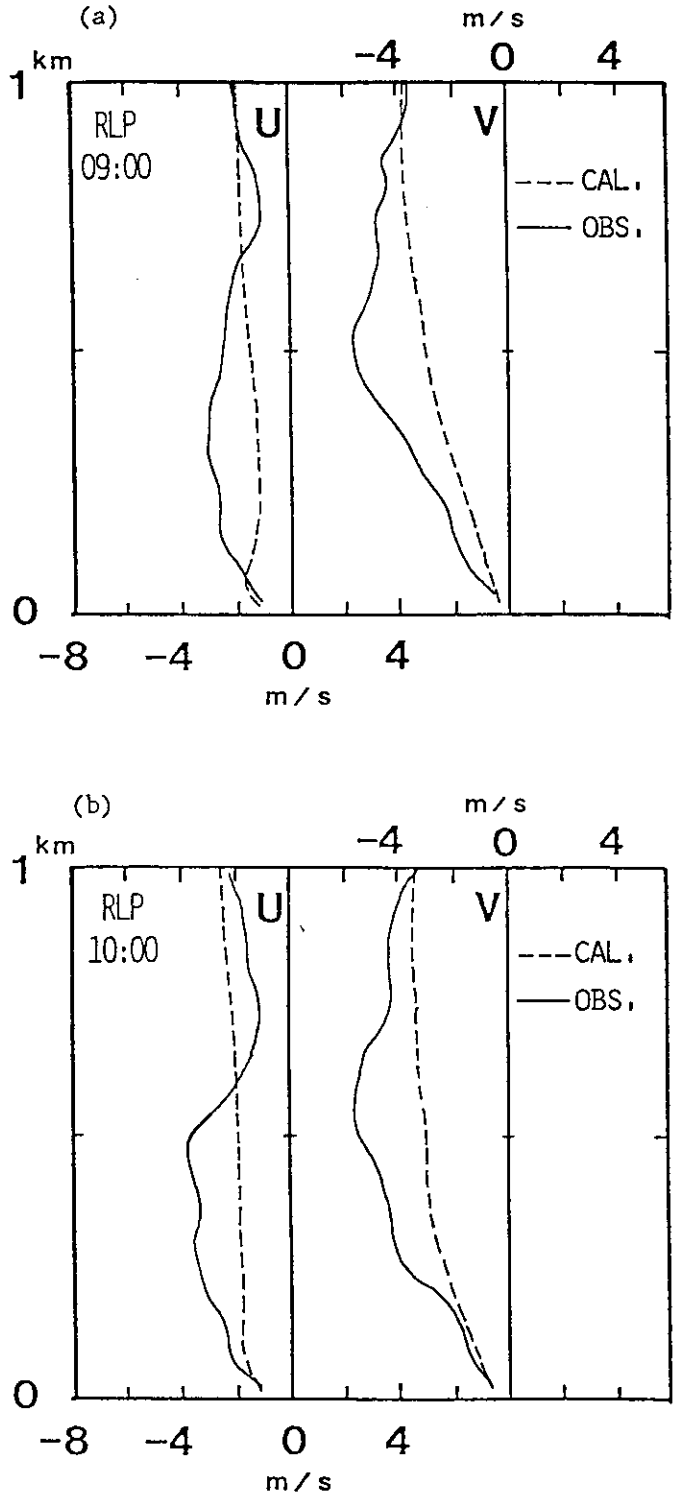

Fig. 7 Vertical profiles of wind speed components u and v at RLP (a through d), SGY (e and f) and OKD (g and h). The observed and calculated wind speed are depicted by the solid and dashed lines, respectively.

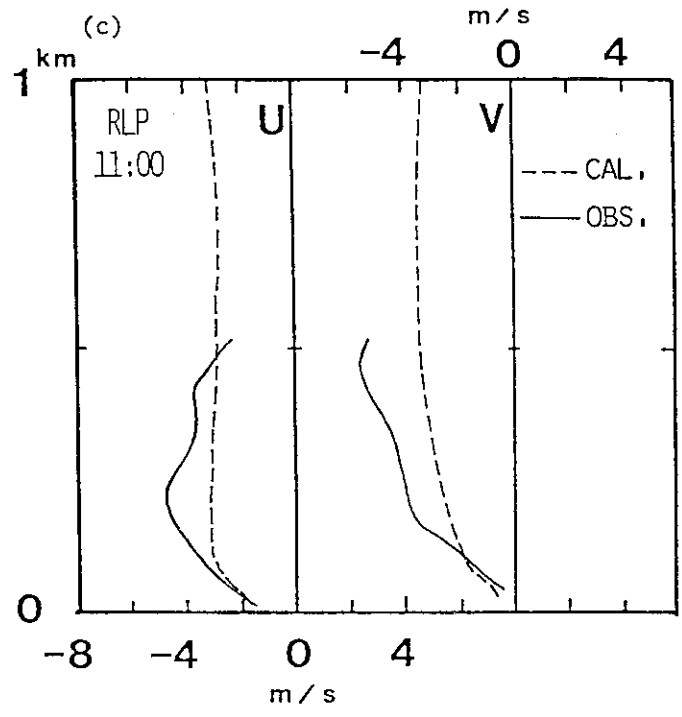

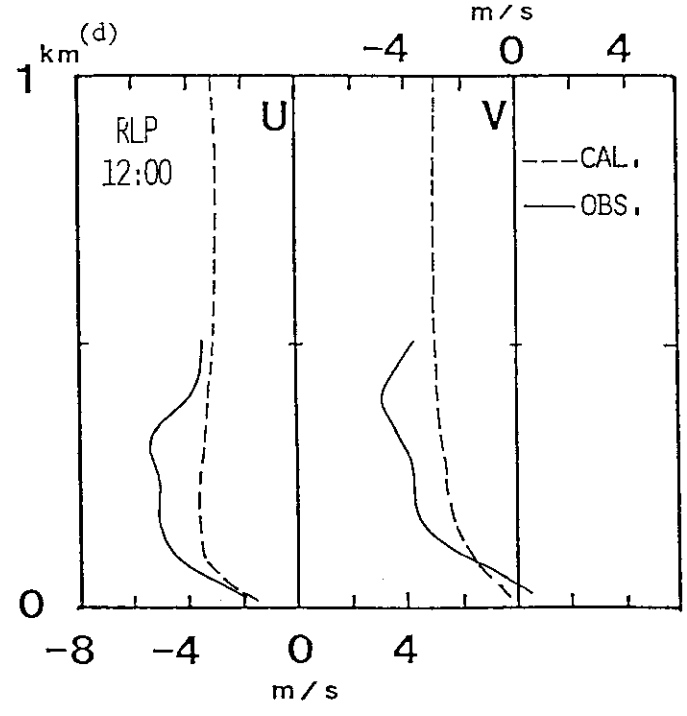

Fig. 7 (Continued)

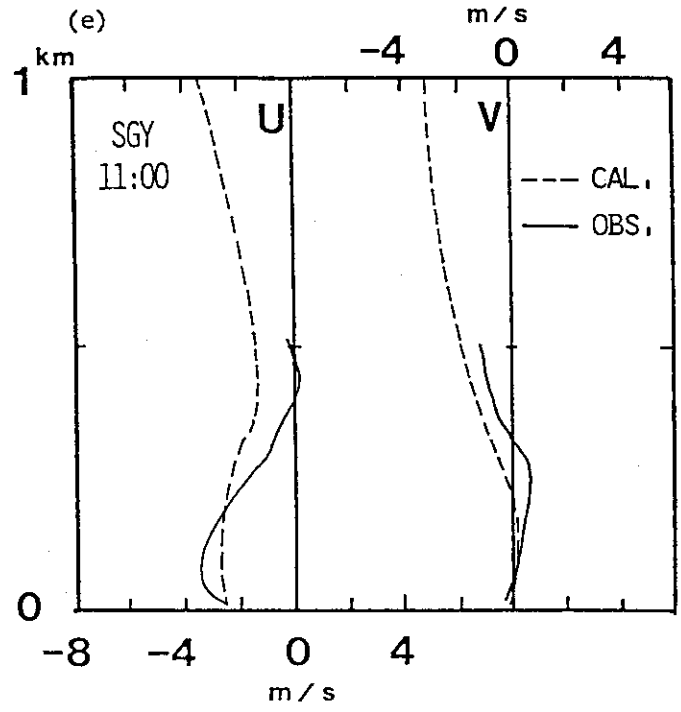

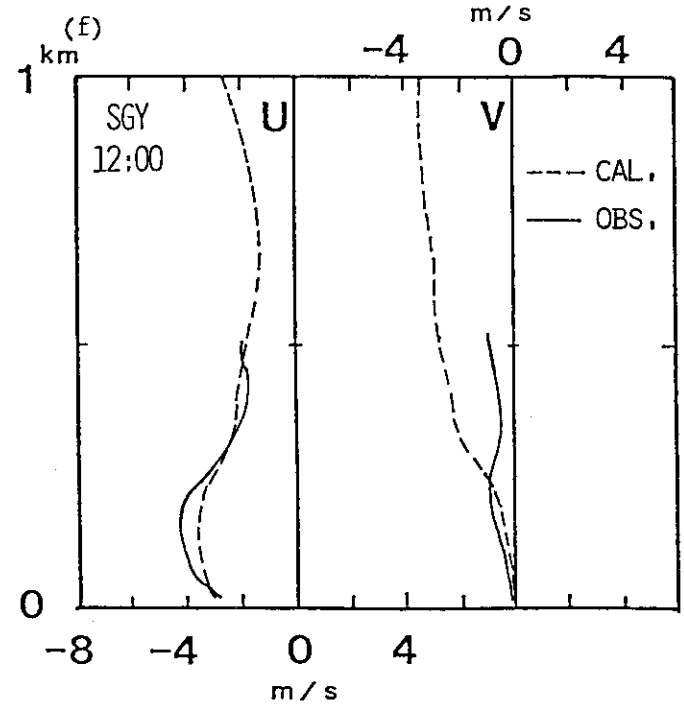

Fig. 7 (Continued)

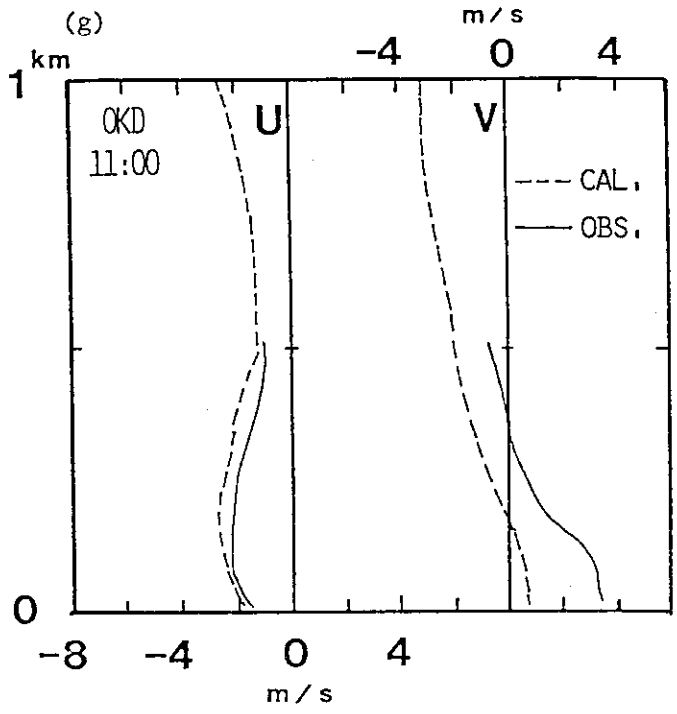

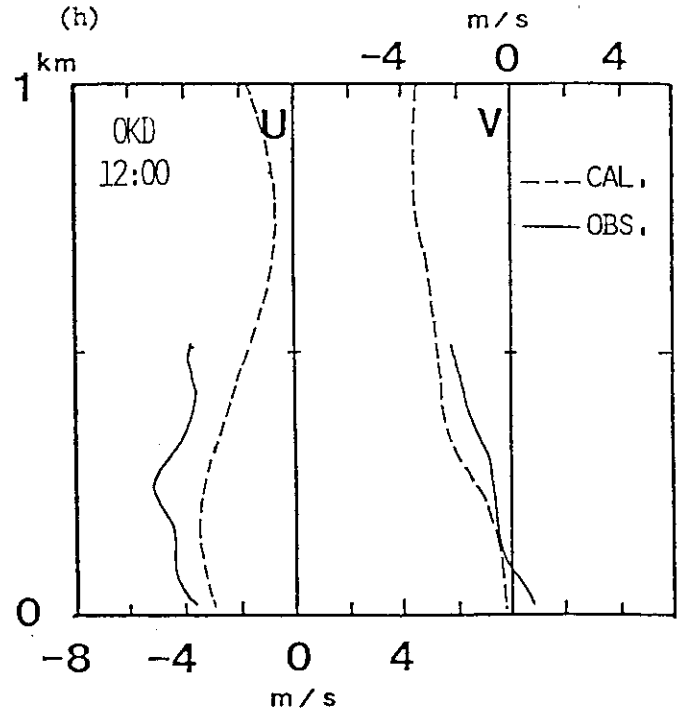

Fig. 7 (Continued)

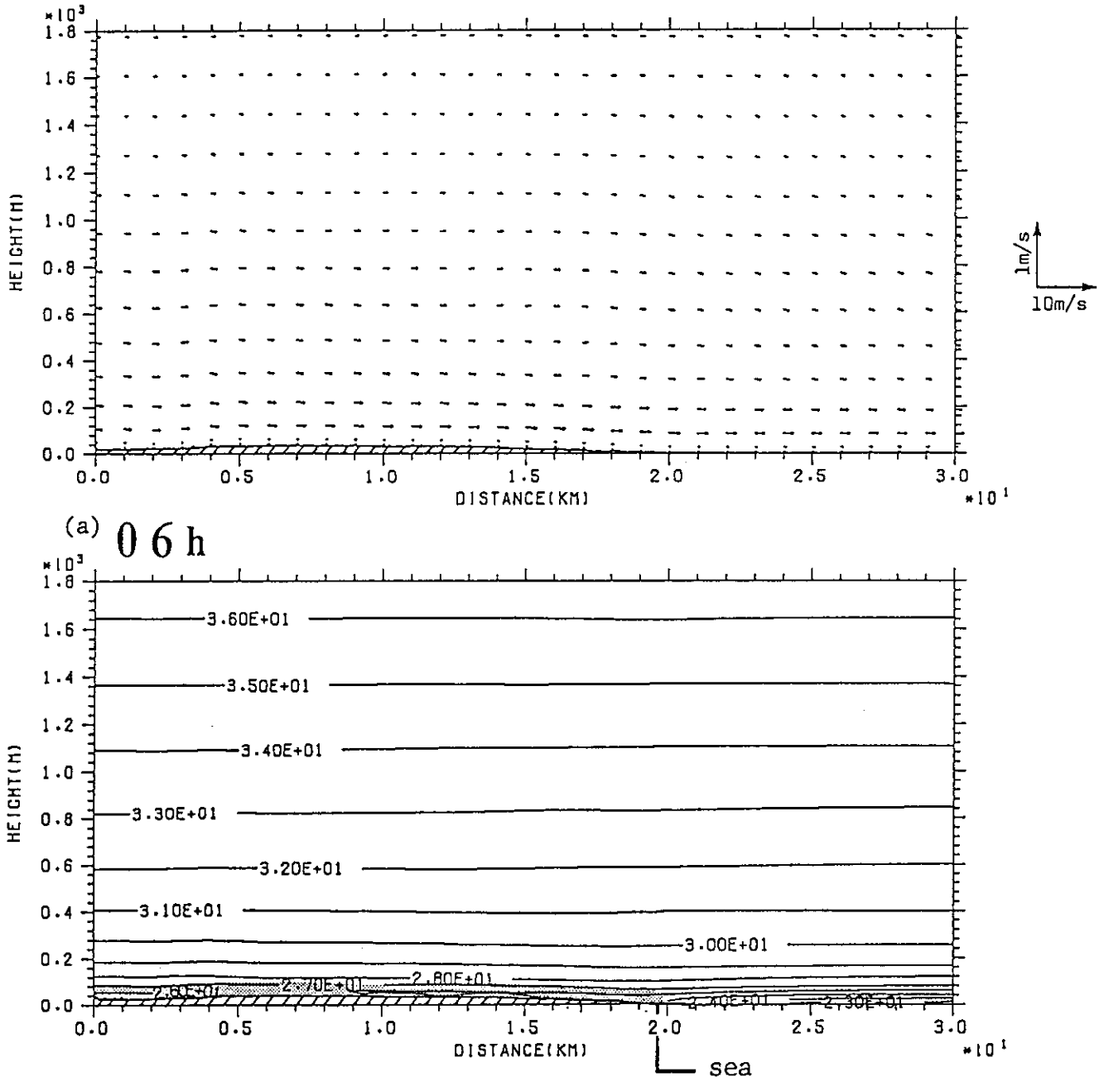

Fig. 8 Vertical structure of wind velocity (u,v), potential temperature θ, and eddy diffusivity K_M in the x-z cross section along the line B in Fig. 1. The coast line is between x=19 and 20 km. The light and thick hatched areas express the regions where $1 \leq K_M < 10$ m^2/s and $K_M > 10$ m^2/s, respectively.

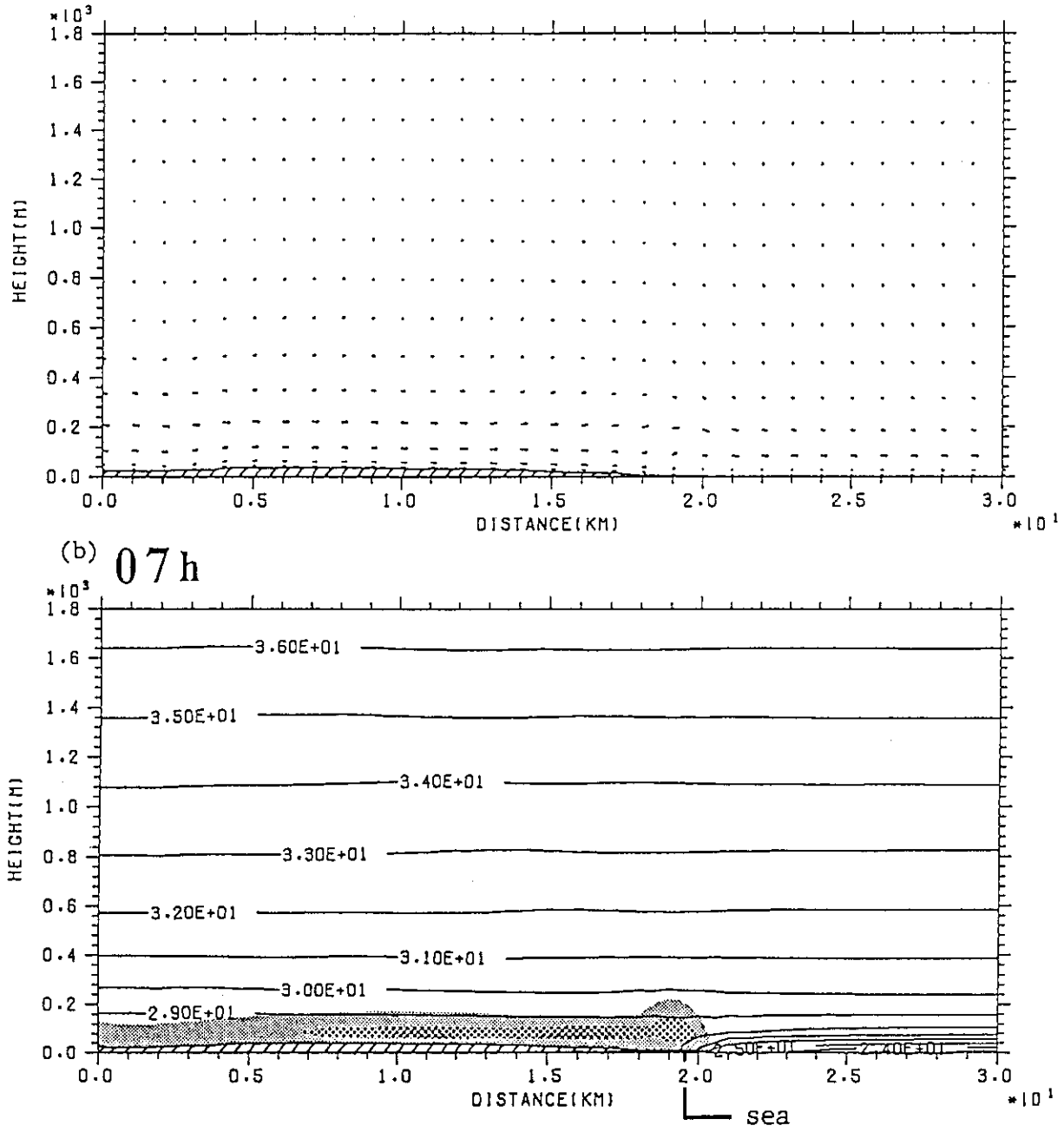

Fig. 8 (Continued)

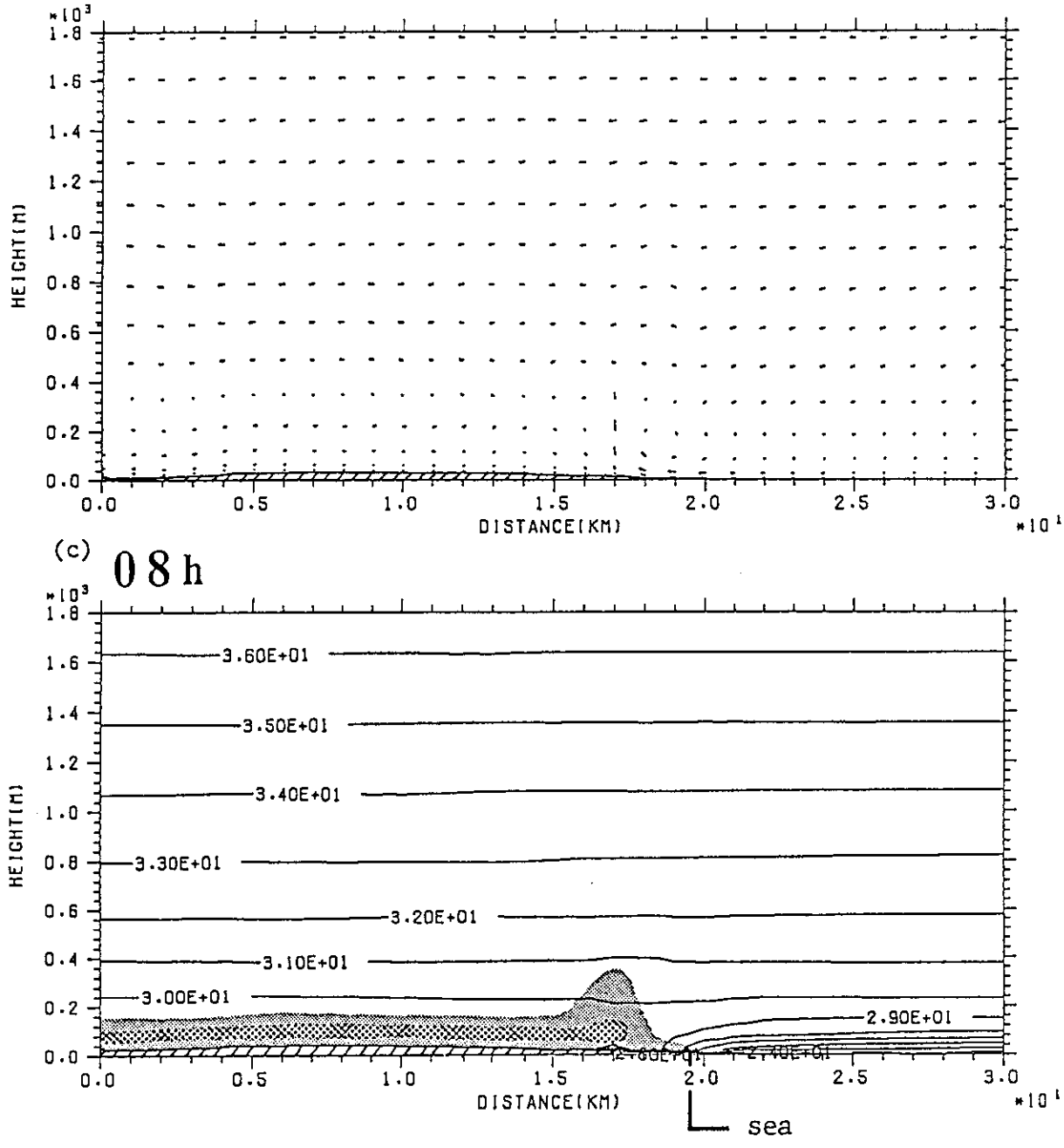

Fig. 8 (Continued)

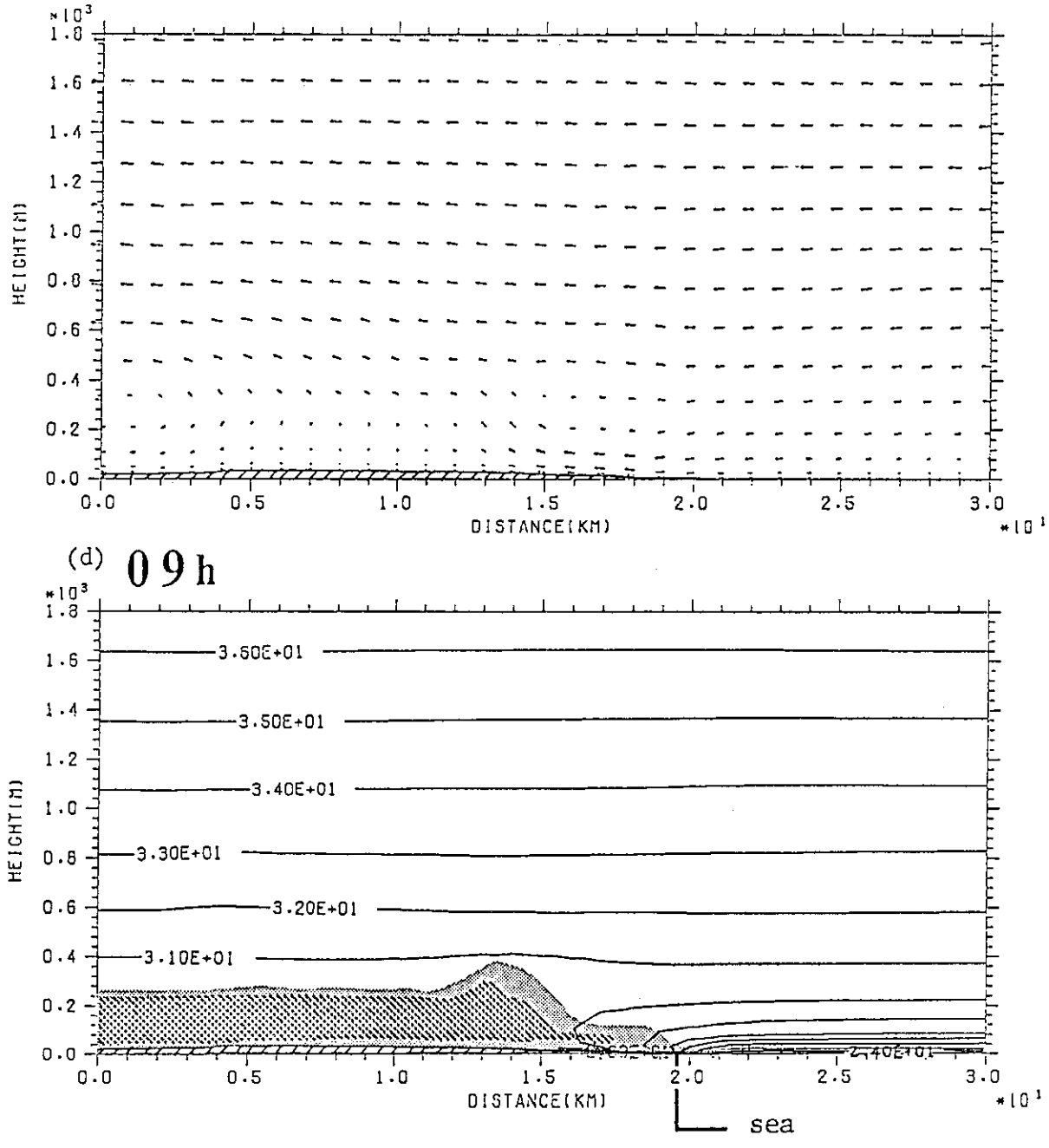

Fig. 8 (Continued)

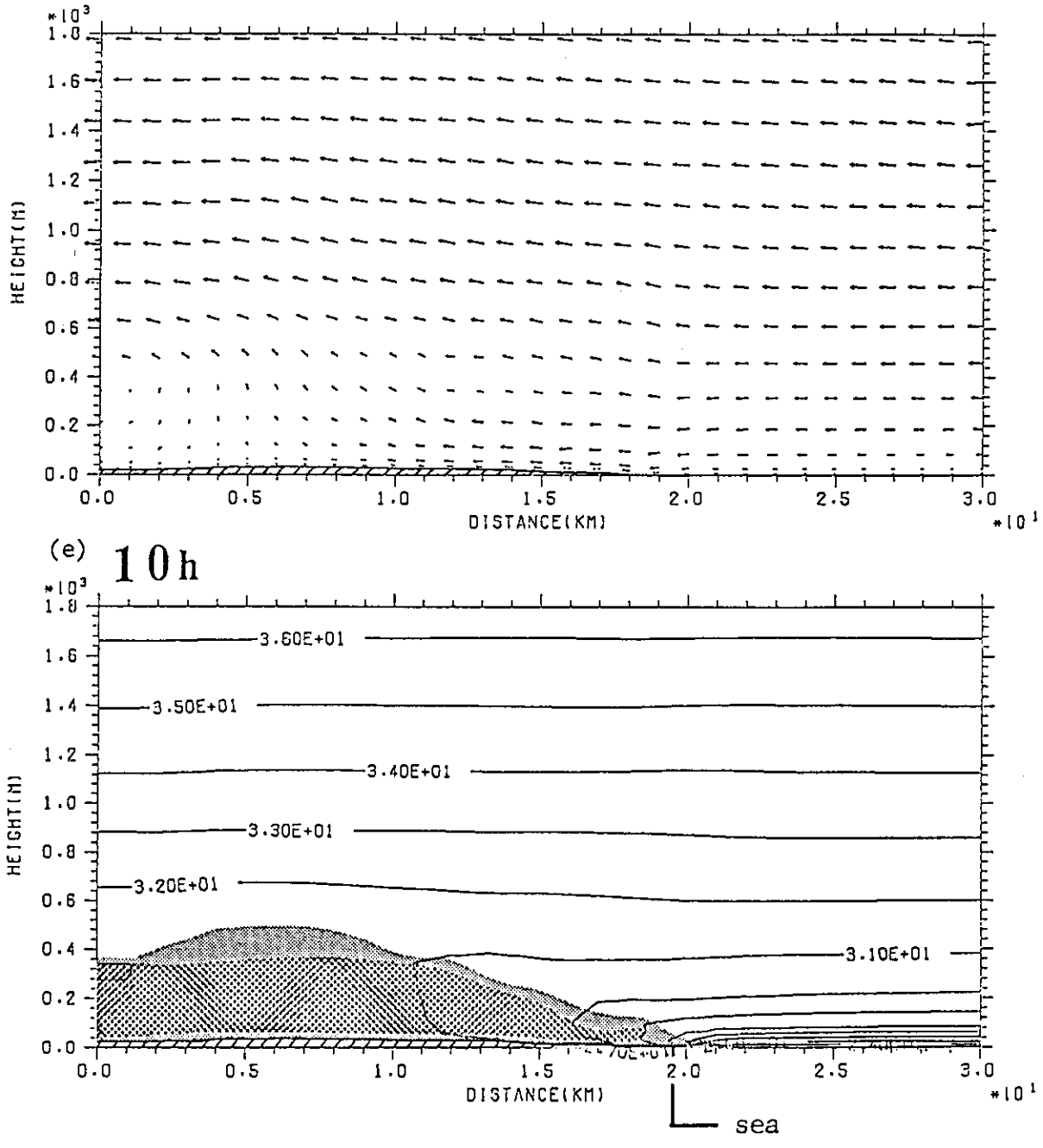

Fig. 8 (Continued)

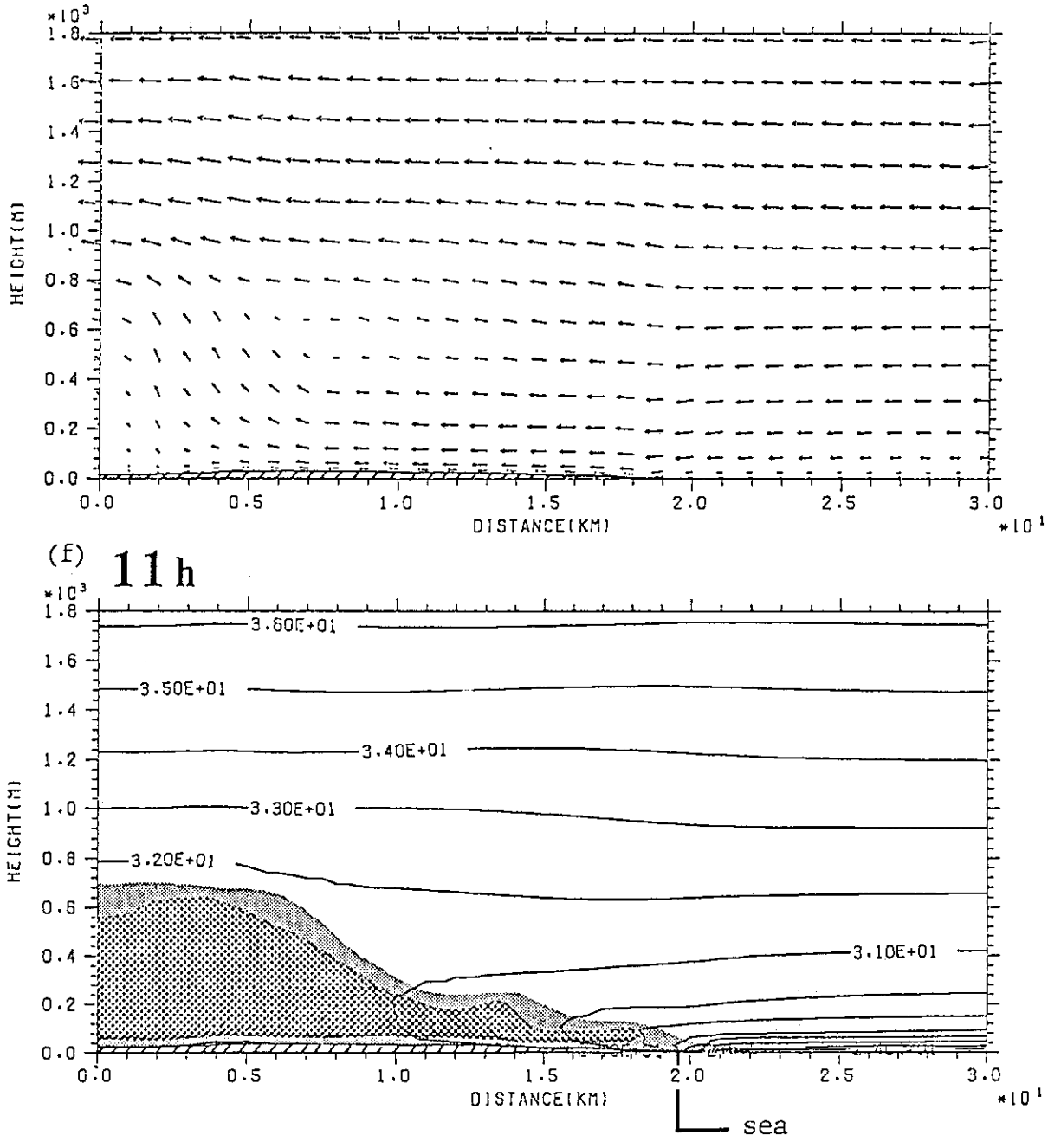

Fig. 8 (Continued)

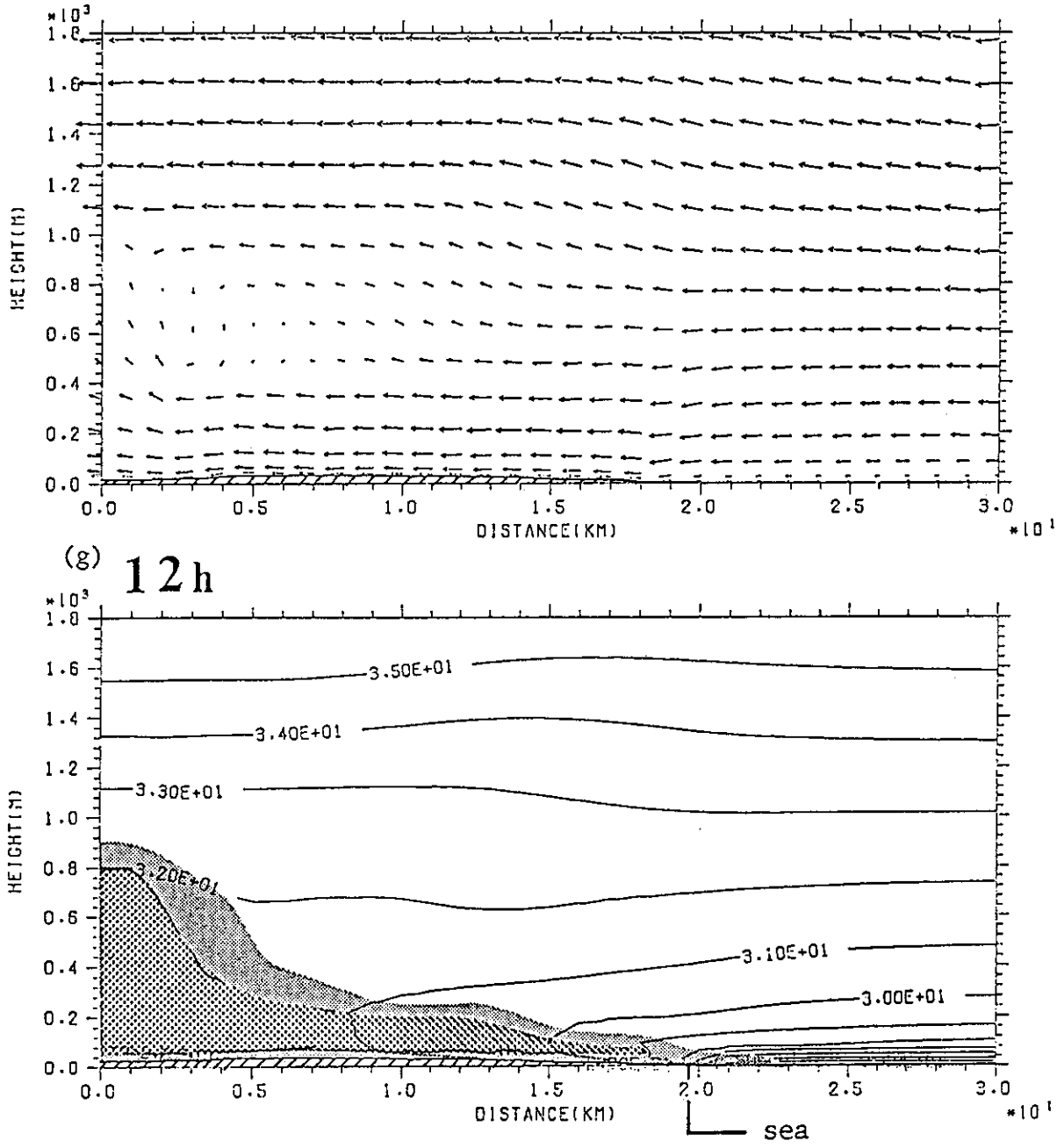

Fig. 8 (Continued)

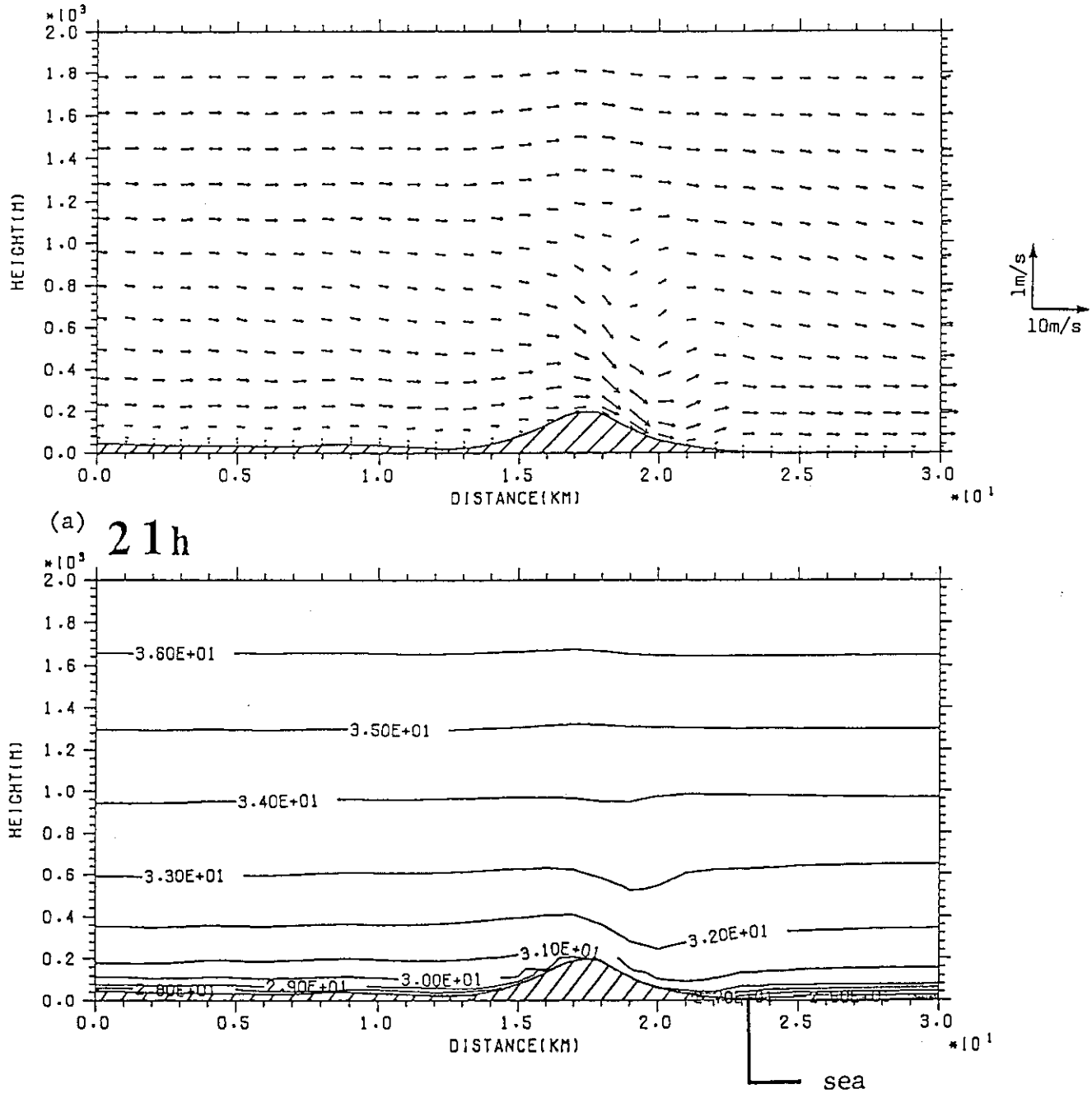

Fig. 9 Same as Fig. 8, except along the line A in Fig. 1 and the coast line is between x=23 and 24 km.

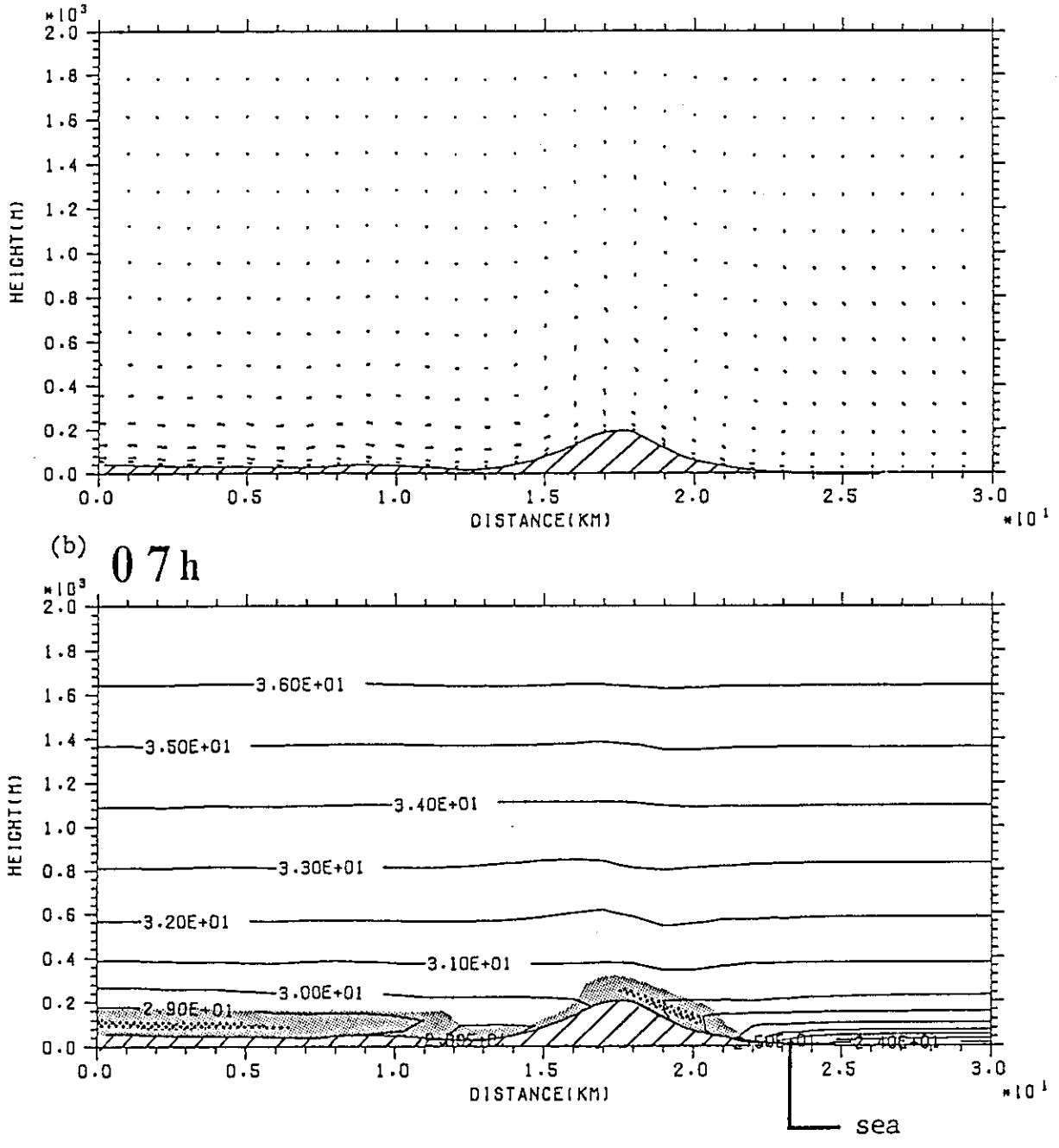

Fig. 9 (Continued)

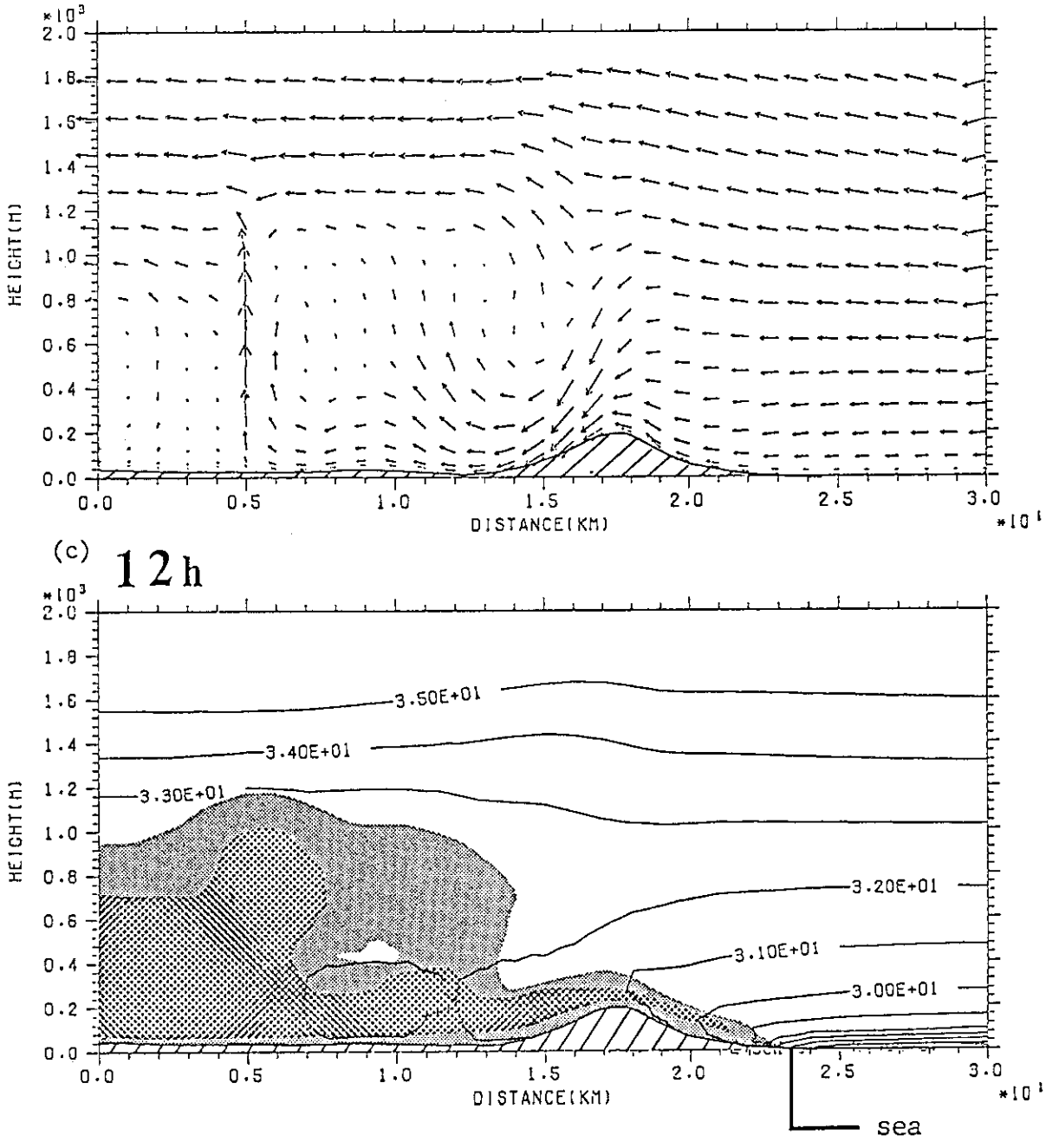

Fig. 9 (Continued)

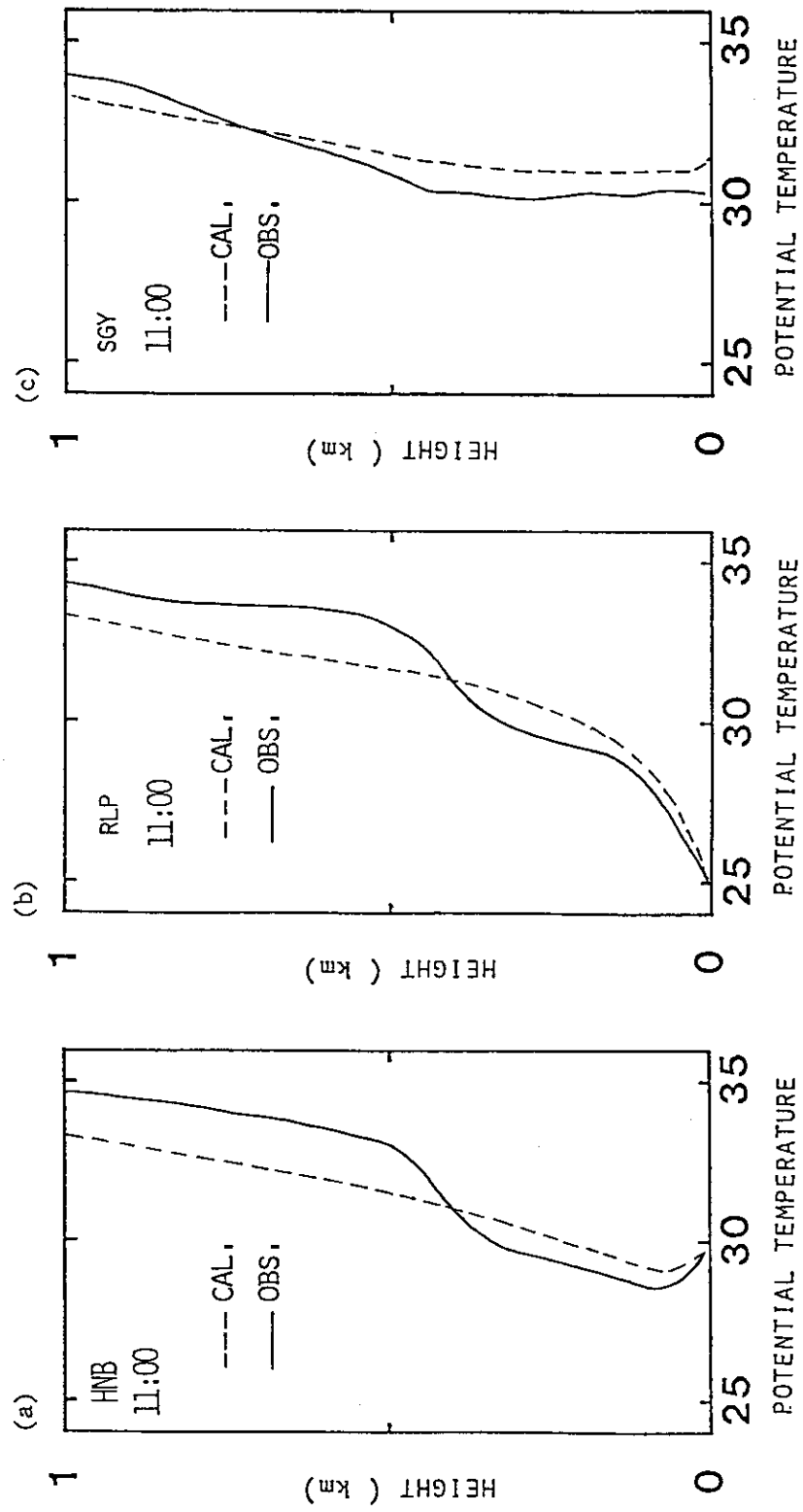

Fig. 10 Vertical potential temperature profiles over (a): HNB, (b): RLP and (c): SGY at 11h JST. The observed and calculated values are depicted by the solid and dashed lines, respectively.

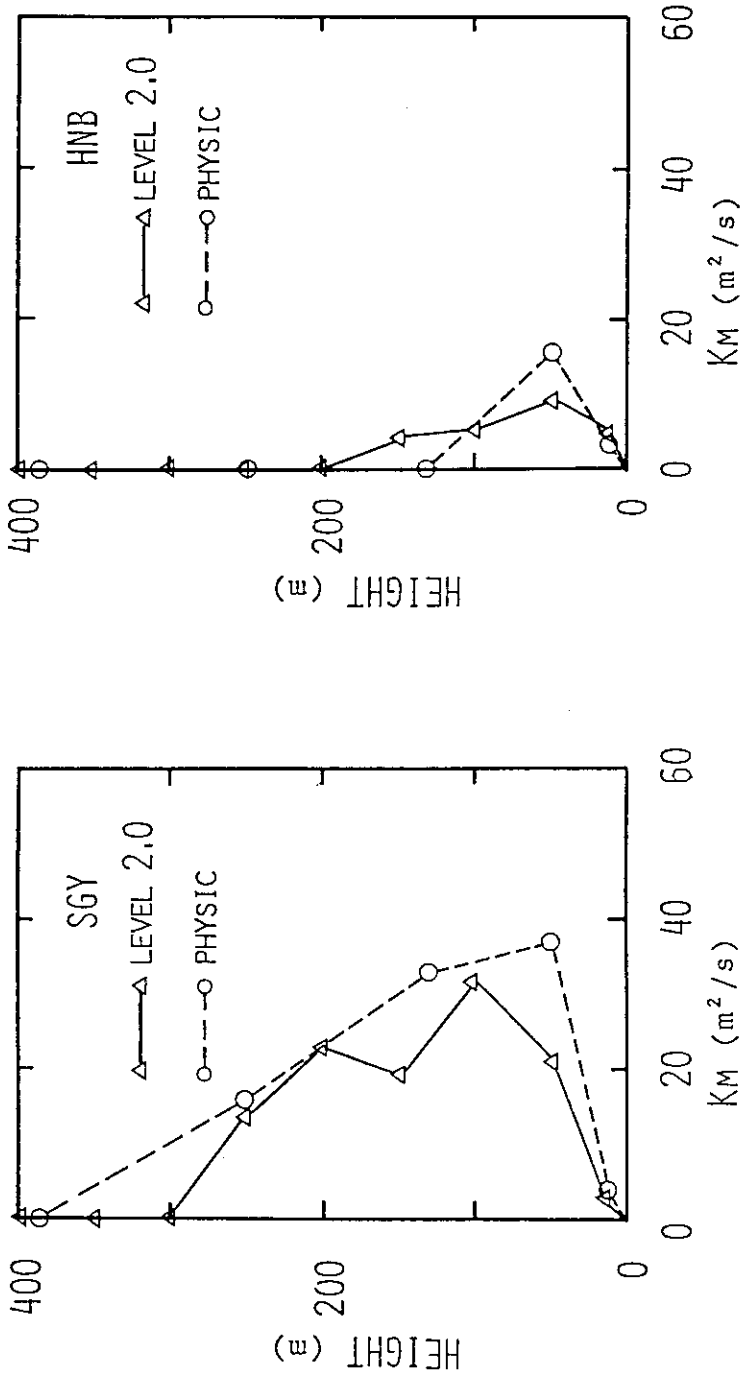

Fig. 11 Vertical profiles of eddy diffusivity K_M over SGY and HNB at 11th JST. The solid lines with triangles depict vertical profiles determined from the observed profiles of wind velocity and potential temperature. The dashed lines with circles depict the calculation result by PHYSIC.